Optimal Siting and Sizing of EV Charging Station Using Stochastic Power Flow Analysis for Voltage Stability

Yuwei Jin, *Member, IEEE*, Moses Amoasi Acquah, *Member, IEEE*, Mingyu Seo, *Student Member, IEEE*, and Sekyung Han, *Member, IEEE*

***Abstract*— Existing literature on planning for electric vehicle charging station (EVCS) fails to consider uncertain factors in power systems, such as load fluctuations and the impact of EV integration. Consequently, using deterministic power flow (DPF) algorithms for EVCS planning is unreliable. To address this, we propose a probabilistic model for EV charging loads and introduce a novel dynamic system voltage stability (DSVS) index. We then present an effective optimization model for EVCS site and size planning using stochastic power flow (SPF). Our model aims to maximize capital gains on investment costs of EVCS, minimize yearly EV users' average wait time and distance to charge costs, and minimize the DSVS index. To simplify the problem, we use the super efficiency data envelopment analysis (SEDEA) method to determine objective weights and transform the multiobjective optimization problem into a single-objective one. Finally, we jointly solve the model using the voronoi diagram and adaptive differential evolution optimization algorithm (ADEOA). We verify the effectiveness of our proposed method using a case study with the IEEE 33-node distribution network topology diagram and a planning area diagram.**

***Index Terms*— Dynamic system voltage stability (DSVS), electric vehicle charging station (EVCS), site and size planning, stochastic power flow (SPF), super efficiency data envelopment analysis (SEDEA), voronoi diagram.**

NOMENCLATURE

i	Electric vehicle (EV) index.
t	Time segment index.
P_t^i, P_{t-1}^i	Charging power of the ith EV at time t and $t-1$.
$\mathrm{SoC}_{\mathrm{exp}}^i$	Expected state of charge (SoC) of the ith EV.
SoC_t^i, SoC_{t-1}^i	SoC of the ith EV at time t and $t-1$.
B_i	Battery capacity of the ith EV.
η	Charging efficiency.
$P^{\max}$	Maximum charging power.
f_1	Annual profit of EV charging station (EVCS).
F^{s}	Annual electricity sales cost.
F^{c}	Annual construction cost.
F^{p}	Annual electricity purchase cost.
F^{om}	Annual operating and maintenance costs.
j	EVCS index.
N_{EVCS}	Total number of EVCS.
$E_{\mathrm{EVCS}}^{j,t}$	Total charging energy of the jth EVCS at time t.
C_{sal}^t	Electricity sales cost at time t.
D	Days per year.
T	Hours per day.
$p_{\mathrm{sl}}^{e,t}$	Expected charging power of the slow EV supply equipment (EVSE) at time t.
σ_{sl}^t	Standard error of the slow EVSE at time t.
$Z_{\partial/2}$	Confidence level value.
$p_{\mathrm{fa}}^{e,t}$	Expected charging power of the fast EVSE at time t.
σ_{fa}^t	Standard error of the fast EVSE at time t.
N_{sl}^j	Number of slow EVSE in the jth EVCS.
N_{fa}^j	Number of fast EVSE in the jth EVCS.
$C_{\mathrm{fix_{cons}}}$	Fixed construction cost.
P_{EVCS}^j	Total construction cost of the EVSE of the jth EVCS.
$C_{\mathrm{cons_{sl}}}$	Construction cost of each slow EVSE.
P_{fa}	Rated charging power of fast EVSE.
$C_{\mathrm{cons_{fa}}}$	Construction cost of each fast EVSE.
C_{land}^j	Land price in the jth EVCS.
r	Discount rate.
o	Payback period.
C_{pur}^t	Energy purchase cost at time t.
$\mho$	Conversion factor.
f_2	EV user's charging convenience.
F^{w}	Annual EV user waiting time cost.
F^{d}	Annual EV user distance traveled to charge cost.
N_{EV}^j	Total number of EVs in the jth EVCS.

Manuscript received 30 September 2022; revised 29 March 2023; accepted 1 May 2023. Date of publication 11 May 2023; date of current version 16 March 2024. This research was supported by Korea Electrotechnology Research Institute (KERI) Primary research program through the National Research Council of Science & Technology (NST) funded by the Ministry of Science and Information & Communications Technology (MSIT) under Grant No. 23A01069. *(Corresponding authors: Moses Amoasi Acquah; Sekyung Han.)*

Yuwei Jin, Mingyu Seo, and Sekyung Han are with the School of Electrical and Electronic Engineering, Kyungpook National University, Daegu 41566, South Korea (e-mail: jinyuwei91@gmail.com; mgseo1218@gmail.com; skhan@knu.ac.kr).

Moses Amoasi Acquah is with the School of Electrical Energy Engineering, Keimyung University, Daegu 42601, South Korea (e-mail: amoasiacquah@gmail.com).

Digital Object Identifier 10.1109/TTE.2023.3275080

τ_{s}	Proportion of EV users choosing slow charging.
T_{s}	Working hours for slow charging mode.
T_{sc}	Average charging duration time for slow charging.
C_{que}	Queuing time cost for EV user which is the average hourly income.
W_{que}^{j}	jth EVCS's average queuing time.
C	EV charging times per day.
τ_{f}	Proportion of EV users choosing fast charging.
ρ	Average utilization for this queueing system which represents the fraction of the service capacity used.
P_0	EVSE idle rate representing the system is empty at any particular time.
λ	Average rate of customer's arrival at the station.
ε	Average system service rate.
T_{f}	Working hours for fast charging mode.
k	Fast EVSE index.
X_j	Abscissa position of the jth EVCS.
Y_j	Ordinate position of the jth EVCS.
x_j^i	Abscissa position of the ith EV in the jth EVCS.
y_j^i	Ordinate position of the ith EV in the jth EVCS.
b	Average EV energy consumption per kilometer.
IP	Injected power vector of node active and reactive power.
G	Power injection function.
U	State vector composed of node voltage amplitude and phase angle.
m, n	Grid node index.
$\Delta W_{m,t}$	Injected active power disturbance of node m at time t.
$\Delta Q_{m,t}$	Injected reactive power disturbance of node m at time t.
$W_{m,t}$	Injected active power of the mth node.
$Q_{m,t}$	Injected reactive power of the mth node.
$U_{m,t}$, $U_{n,t}$	Voltages of the nth and the mth node at time t, respectively.
N_{node}	Total number of nodes.
G_{mn}	Real part of the nodal admittance matrix.
δ_{mn}	Phase angle difference between node m and n.
B_{mn}	Imaginary part of the nodal admittance matrix.
$\Delta U_{m,t}$	Voltage disturbance at node m at time t.
J_t	Jacobian matrix at time t.
$\Delta W_{m,t}^{\mathrm{L}}$	Baseload disturbance of the mth node at time t.
$\Delta W_{j,m,t}^{\mathrm{EVCS}}$	Charging power disturbance of the jth EVCS on the mth node at time t.
B_m^j	Boolean value, value is 1 when j connect into the mth node, else it is 0.
$W_{m,t}^{\mathrm{e}}$	Expected value of node injected power of the mth node at time t.
$W_{m,t}^{\mathrm{L}}$	Expected value of baseload of the mth node at time t.
$W_{j,m,t}^{\mathrm{EVCS}}$	Expected charging power of the jth EVCS on the mth node at time t.
$U_{m,t}^{\mathrm{e}}$	Expected value of node voltage of the mth node at time t.
X	Random variable.
l	Raw moment order index.
$a^l(X)$	lth-order raw moment of X.
h	Random variable index.
p_{h}	Probability of $X = x_{\mathrm{h}}^l$.
x_{h}^l	Discrete point data in the lth order.
$K^l(\Delta W_{m,t})$	lth-order cumulant of the injected active power of the mth node at time t.
$K^l(\Delta U_{m,t})$	lth-order cumulant of the node voltage of the mth node at time t.
μ	Mean value.
$C^l(\Delta U_{m,t})$	Coefficient of the lth-order cumulant of the node voltage of the mth node at time t.
$\varphi^l(\Delta U_{m,t})$	lth derivative of the standard normal distribution function with respect to $\Delta U_{m,t}$.
I^{DSVS}	Dynamic system voltage stability (DSVS) index.
$U_{m,t}^{\mathrm{upp}}$	Upper voltage boundary of the mth node at time t.
$U_{m,t}^{\mathrm{low}}$	Lower voltage boundary of the mth node at time t.
U^{N}	Nominal voltage.
$\wp_{m,t}$, $\mathfrak{z}_{m,t}$ $\xi_{m,t}$, $\varrho_{m,t}$	Slack variable.
f_3	System's minimum dynamic voltage stability index.
s	Output index.
z	Input index.
v	Decision-making unit (DMU) index.
$\beta_{v,z}$	Weight coefficient of the zth output value of the vth DMU.
$y_{v,z}$	zth output value of the vth DMU.
$\alpha_{v,s}$	Weight coefficient of the sth input value of the vth DMU.
$x_{v,s}$	sth input value of the vth DMU.
ϑ_v	Efficiency value of the vth DMU.
ω_1, ω_2, ω_3	Weight coefficients.
$\beta_{v,1}$	Weight coefficient of the output of the vth DMU.
$\alpha_{v,1}$, $\alpha_{v,2}$	Weight coefficients of the input of the vth DMU, respectively.
$\max\ f_1$, $\min f_2$, $\min f_3$	Fixed values with respective optimal solutions without considering the other two objective functions.

$f_{v,1}$, $f_{v,2}$, $f_{v,3}$	Optimal solutions obtained by the optimization algorithm after the vth input and output weight vector.
$U^{\min}$	Minimum values of the node voltage amplitude.
$U^{\max}$	Maximum values of the node voltage amplitude.
$P_{m,t}^{\max}$	Maximum access power allowed by the mth node at time t.
$R_{\max}$	Maximum EVCS service radius.
$W_q^{\max}$	Maximum waiting time.
P_{sl}	Rated charging power of slow EVSE.
$d(x, G_u)$	Euclidean distance between x and G_u.
$d(x, G_j)$	Euclidean distance between x and G_j.
G_u, G_j	Location of the uth and the jth EVCSs.
x	Location of each EV.

I. Introduction

DUE to weather and battery technology limitations, the actual cruise range of most EVs on the market is between 70% and 80% of the standard operating range. In some cases, it may be less than 50%, which easily affects drive mileage, causing charging anxiety, negative purchase intention, and consumption enthusiasm of potential EVs customers [1], [2]. Due to the current economic and technical factors, it is difficult to make substantial progress in battery life in the short term. Therefore, to promote EV development, it is necessary to build sufficient EVCSs. However, under the current national EV stimulus subsidy policy, many stakeholders build EVCSs and EVSEs without comprehensive planning. This act ignores essential factors such as the consistency between layout, infrastructure location, and the distribution of charging demand, thus resulting in a low average utilization rate of EVSE of about 4% [3]. Because of this, it is necessary to build an optimization model for the site and size planning of EV charging facilities to improve the construction of the charging infrastructure service network.

Planning the site and size of EVCSs involves multiple stakeholders. These stakeholders comprise EVCS owners and operators, property owners and managers, EV manufacturers, government agencies, utility companies, or distribution companies (DisCos). Among these groups, charging station ownership and operation can be attributed to EV manufacturers, utility companies, and individuals and companies involved in managing and owning the charging stations.

At present, the factors researchers consider when creating an optimization model for siting and sizing planning of EVCSs is incomplete. Some studies, such as those referenced in [4] and [5], consider the fixed cost of charging station construction and the cost of transportation charging to minimize the total yearly cost. The balance of power flow is considered the constraint to building an optimal allocation algorithm of EVCSs. Ugirumurera and Haas [6] present a methodology to determine the optimal resource size that minimizes the charging system's investment costs. Yan and Ma [7] formulate the optimal component sizing problem of the charging station to mitigate the entire system's economic cost. Hussain et al. [8] determine the optimal energy storage system (ESS) capacity using the annualized ESS cost, penalty cost for buying power during peak hours, and resilience violations. Luo et al. [9] and Zhou et al. [10] propose an optimization model to jointly deploy EVCSs and distributed generation (DG) resources by minimizing annualized social costs, i.e., investment, operation, fuel and carbon emission, purchase of electricity, and EV battery degradation. Duan et al. [11] propose a collaborative planning method for the distribution network of EVCS. The upper model sets the charging station's capacity to maximize the annual social comprehensive benefit, and the lower model sets the charging station's location to minimize the distribution network planning cost. Guo et al. [12] propose a multiobjective EVCS planning model to minimize pollutant costs (PM10, SO_2, NO_x, and CO_2) and social costs. However, these studies only consider the interests of operators, ignoring the impact of EV users' convenience and the power grid's reliability on EVCS planning. Most EV users prefer to charge their vehicles based on the proximity principle in real life, which means the layout of charging stations will affect the spatial distribution of EV charging requirements. Additionally, if only social costs are considered, it can negatively impact the reliability of power grid operation. There is a mutual coupling relationship between these three factors (operator interests, EV user convenience, and the reliability of power grid), and neither is indispensable.

Ji et al. [13] proposed an approach to efficiently determine the locations and sizes of solar energy-assisted charging stations for an urban area. The approach considered construction cost, solar energy fluctuation, and user requirements. Parastvand et al. [14] modeled the traffic flow over the EV network as a complex network and used figure properties to determine the optimal site and size for EVCSs, which minimized waiting times at the charging stations. Chen et al. [15] developed an algorithm that determined the charging station location by minimizing the travel cost of EV users, while the maximum charging load of the charging station in a week determined the capacity. Liu and Bie [16] proposed an allocation model that minimized the annual cost, which included the charger investment cost, land purchase cost, grid reinforcement cost, and EV user queuing time. Ren et al. [17] formulated an EVCS allocation problem that minimized the construction and operation cost and the wastage cost in EV user charging. Zhu et al. [18] addressed the EVCS location and sizing problem by minimizing the EVCS's cost (installing cost and management cost) and the EV user's cost (station access cost and charging a cost). Although these references consider the interests of operators and EV users, they fail to address the impact of charging stations on the stability of grid operation. Large-scale EV operations can inevitably impact the grid's operation and, in severe cases, cause grid collapse. Therefore, the planning of the charging station and its impact on the grid must be considered.

Deb and Gao [19] formulate the EVCS placement problem by minimizing the social cost, penalty paid cost for voltage deviation, and travel time cost. Hashemian et al. [20] propose a mixed-integer linear programming model that considers the social cost, queueing, and travel cost, cost of installing volt-ampere (VA) capacity for stations, and costs

of purchasing active and reactive power from the upstream network to solve the fast charging station's allocation problem. Zhang et al. [21] propose a multicriteria-oriented method for efficiently deploying EVCS infrastructure to solve the nondeterministic polynomial (NP)-complete problem by minimizing queueing time and grid loss. Erdinc et al. [22] propose a method to plan the optimal location of EVCSs with maximum capacity by considering the safety and stability of the distribution network. Wang et al. [23] present a multistage collaborative planning model for the coupled EVCS infrastructure and power distribution network to minimize the distribution system's investment cost and energy loss while maximizing the annually captured traffic flow. Awasthi et al. [24] present an optimal placement strategy of EVCS by considering the construction cost of EVCS and grid power quality parameters. In [25], an optimization-based algorithm is proposed to specify the optimum size of the storage system in the charging station by minimizing the cost of the storage system and the impacts of station operation on the power grid. Henrique et al. [26] formulate a two-stage approach to minimize the grid loss and maximize the proximity of charging stations to the load centers. Although the above literature considers investors, EV users, and the power grid at the same time, it ignores uncertain factors in the system. In real life, numerous uncertainties exist in existing power grid systems, such as the randomness of system parameters, load profiles, and EV user charging behavior, and these uncertainties can significantly impact the results of EVCS planning.

Zeb et al. [27] use the arrival time, departure time, and traveled distance of EVs to build a probabilistic model of charging behavior and select the location of the EVCS with the objective function of minimizing the social cost and grid loss cost. Amini et al. [28] and Kazemi et al. [29] proposed an approach for simultaneously allocating distributed renewable resources (DRRs) and EV parking lots by minimizing grid loss and cost. The authors considered the capacity credit of DRRs and parking lot hourly electricity demand. Fan et al. [30] modeled DG and load uncertainties and proposed an optimal integrated distribution plan by considering social cost, PV and wind operation cost, power loss, and carbon emission cost. The literature above considers system uncertainty but uses deterministic power flow (DPF) calculation to solve the problem, which cannot fully reflect the system's operation and will affect the robustness of the planning model. Therefore, research on stochastic power flow (SPF) algorithms for power system analysis is crucial. SPF estimation not only considers the probability distribution of random variables and parameters in the network during power flow design and the influence of load randomness on the power grid's operation state, but also can obtain more abundant information, such as node voltage and line power flow expectation and standard deviation values and distribution intervals. This information can provide a reference basis for assessing the operation risk of the power grid and making planning and development decisions. Hence, the results obtained using SPF are more realistic and reliable than the results of DPF.

Currently, very few literature pieces use SPF to solve charging station planning, most of which are used to analyze the impact of various renewable energy sources on the power grid. In [31], a multiobjective problem is proposed by considering energy loss, voltage deviation, and land cost to determine the EVCS location. The uncertainties of EV have been considered in this work using the 2-m point estimation method (2PEM). Although 2PEM is easy to calculate and implement, its calculation accuracy is low, and it has a certain level of computational complexity when dealing with the time and space correlation of input variables, which affects the robustness of charging station planning. In [32], an SPF analysis method is proposed to evaluate the impact of uncertainties on the power flow of microgrids (MGs). Zhang et al. [33] use the SPF algorithm to consider the random characteristics of DG and evaluate the influence of DG on the voltage quality of the distribution network. In [34], an SPF framework for optimal operation is proposed to be solved by the Monte Carlo simulation (MCS) method, considering generation cost as an objective. Lin et al. [35] use a Nataf transformation-based unscented transformation (UT) to conduct probabilistic analysis for an autonomous hybrid ac/dc MG. Wei et al. [36] analyze the impact of large-scale wind power on the grid's voltage limit and flow distribution based on an SPF algorithm. Li et al. [37] aim to study the impact of future load demands and rooftop PV on the existing power network via SPF.

Most charging station planning problems involve multiple objectives, which are often simplified into single-objective problems using techniques such as the linear weighting method [38], the ideal point method [39], or the objective function method [40]. The appropriate weight coefficient plays a crucial role in achieving optimal results. For instance, Jing et al. [41] used the ε-constraint approach to identify the nondominated optimal solution set for multiobjective optimization. They also developed a comprehensive evaluation model combining analytic hierarchy process (AHP) and gray relational analysis (GRA). The proposed evaluation model considers different criteria from various perspectives and scales to assess the system performance. However, some existing studies, such as [42] and [43], have used subjective weight selection methods like AHP and hesitant fuzzy independent judgment (HFIJ) for multiobjective analysis. These methods lack objectivity and may not be appropriate for charging station planning models. Using the weighted sum method and fuzzy control, Villaobos et al. [44] proposed a multiobjective optimization method for vehicle-to-grid (V2G) scheduling. However, this approach relies heavily on expert knowledge and intuition, which may lead to inconsistencies or biases if decision-makers' assumptions or knowledge are incorrect or incomplete. Similarly, Bitencourt et al. [45] used hierarchical clustering to define charging station service zones based on EV owners' locations. However, this method lacks a straightforward method to determine the optimal number of clusters, which requires empirical decisions that may affect the accuracy of the resulting clusters. Liu et al. [46] proposed a multiobjective charging station location model that integrates an improved multiobjective particle swarm optimization (MOPSO) process and an entropy weight-based evaluation process. Although simple, this method may lead to weight distortion and produce valid results. This article proposes a

super efficiency data envelopment analysis (SEDEA) approach to overcome this limitation in selecting weight coefficients. SEDEA considers the weight of each input and output of the DMU as a variable and evaluates it from the perspective that is most beneficial to the DMU. Unlike other methods, SEDEA does not rely on assumptions or subjective human factors, which makes it more reliable.

To address the issues outlined above, we propose a comprehensive optimization framework for planning the size and location of EVCSs. This model considers the profit of the EVCS operator, the convenience of EV users, and the stability of the power grid, utilizing SPF to account for uncertainties in both EV charging and overall grid demand. The key contributions of this article can be summarized as follows.

1) By considering both static and dynamic information regarding EVs, we have developed separate probability models for fast charging loads and slow charging loads, thus enabling a more practical approach to construct charging station models.
2) Our framework is designed to achieve the following objectives.
   a) *Utility Operator Benefits*: We have developed an objective function that maximizes the difference between yearly revenue and investment cost of EVCSs, considering operator benefits.
   b) *EV User Convenience*: We have also developed an objective function that minimizes the yearly average of EV user waiting time and distance cost.
   c) *Considering System Uncertainties*: We account for randomness in the distribution network by combining cumulants and Gram–Charlier expansion methods to evaluate dynamic SPF, incorporating both baseload and EVCS load. We have also proposed a DSVS index to analyze and improve the grid's stability and established an objective function based on the index.
3) To choose the most effective weights for each objective function in our optimization model, we have employed the SEDEA. Additionally, we have used the linear weighted sum method to transform the multiobjective problem into a single-objective problem, thus resulting in improved optimization results.

The rest of this article is organized as follows.

Section II describes the process of building a probabilistic model of EV charging load. Section III describes the mathematical optimization model of EVCS siting and sizing plan and the SEDEA method. Section IV describes the joint solution method combing the voronoi diagram and adaptive differential evolution optimization algorithm (ADEOA). Case study and simulation results are discussed in Section V. Section VI summarizes findings and conclusions.

II. EV Charging Load Probabilistic Modeling

The development of an allocation model for EVCSs heavily relies on the accuracy of the EV charging load probability model. However, as the EV market is still in the early stages of development in many countries, a limited amount of EV data is available for research. Most literature in this field only builds charging load models based on EV user travel activities, which may not accurately reflect real-world scenarios. Therefore, this article proposes a more practical and comprehensive approach for building a probabilistic model of EV charging load.

TABLE I
EV Information

Brand	Model	Battery capacity(kWh)	Brand sales Rate (%)
Mi	i-MiEV	16	0.23
Smart	ED	17.3	1.18
Chevrolet	Spark EV	18.3	1.19
Honda	FIT	20	0.16
Fiat	500e	24	4.28
Honda	Clarity	25.5	0.33
BMW	i3	27.2	5.98
Mercedes	B250e	28	0.68
Ford	Focus-e	33.5	1.38
VW	e-Golf	35.7	2.16
Hyndai	Ioniq-e	38.3	0.13
Nissan	LEAF	40	17.73
Toyota	RAV4	41.8	0.37
Chevrolet	Bolt EV	60	6.75
Kia	Soul EV	64	1.03
Tesla	Model 3	78	22.8
Tesla	Model S	100	23.02
Tesla	Model X	100	10.6

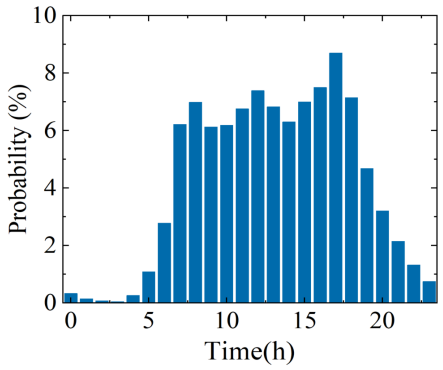

Fig. 1. Hourly plug-in time PMF.

Step 1: Collection of each EV's battery information, which is mainly divided into static information and dynamic information:

The static information of an EV mainly includes the model type, battery capacity, and maximum charging power. Table I provides the necessary data for the first two pieces of information, and the EV model and battery capacity for each EV will be randomly generated according to the sales rate in Table I [47]. The maximum charging power for an EV is determined by the charging mode the EV user selects, which is either 50 or 7 kW.

On the other hand, the dynamic information of an EV involves the plug-in time, parking duration time, and initial SoC. In [47], probability mass function (PMF) models for these three pieces of information were developed using Federal Highway Administration (FHWA) data, as presented in Figs. 1–3. Based on these PMF models, the charging behavior of each EV is predicted using the Monte Carlo method.

Step 2: Using the obtained information of each EV, calculate the uncoordinated charging load profile of each vehicle. Uncoordinated EV charging refers to charging immediately after

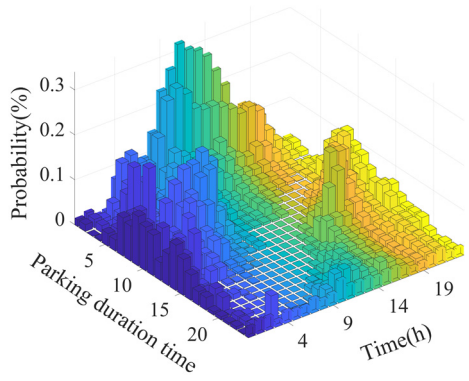

Fig. 2. Hourly parking duration time PMF.

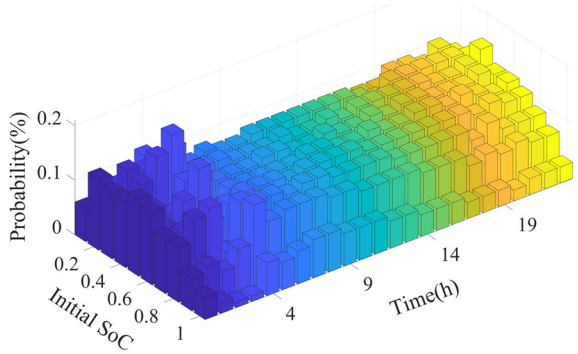

Fig. 3. Hourly initial SoC PMF.

arriving at the destination and stopping when fully charged. During the entire charging process, it is directly charged at the maximum allowable charging power until completion. The charging power of each vehicle during the noncharging period is 0, and the charging power during the charging period is

$$P_t^i = \min\left(\frac{\left(\mathrm{SoC}_{\exp}^i - \mathrm{SoC}_t^i\right) \times B_i}{\eta}, P^{\max}\right) \tag{1}$$

$$\text{S.t. } \mathrm{SoC}_t^i = \mathrm{SoC}_{t-1}^i + \frac{P_{t-1}^i \times \eta}{B_i}. \tag{2}$$

Step 3: Repeat Step 1–Step 2 to generate the most charging load profiles for EVs, which is set to 50 000 times in this article.

Step 4: This article assumes that the EV charging load follows a normal distribution. The mean and standard deviation of the EV charging probability distribution in each period are calculated using the obtained EV charging power of all EVs during that period.

III. Mathematical Model

The planning of EVCSs is a complex endeavor that requires consideration of multiple factors. If operators prioritize cost reduction, they may construct a limited number of EVSEs, thus resulting in inconvenience to EV users and longer waiting periods. Conversely, building a large number of EVSEs to generate more revenue can reduce users' waiting times, but it may also overload the grid and lead to potential collapse. Nevertheless, constructing a large number of EVSEs can also lead to the underutilization of services, thus resulting in losses. It is clear that the overall profits of EVCSs, EV users' convenience, and grid reliability are interdependent and must be considered together when planning EVCSs. Hence, this article considers both the overall profits of EVCSs, EV users' convenience, and grid reliability and establishes a multiobjective optimization model to plan the siting and sizing of EVCSs. The siting process involves identifying the best location for EVCS, while sizing determines the number of fast and slow EVSEs that each station can accommodate. To determine the importance of each objective function, we employ the SEDEA method and use the linear weighted summation method to transform the multiobjective programming model into a single-objective one. The optimal planning scheme for the final EVCS is then determined through optimization. By using a comprehensive approach, we can ensure that the final plan optimizes all three factors to create a well-functioning and efficient charging station for EV users.

A. Annual Profit of EVCS

The installation of EVCSs hinges on supporting infrastructure development, necessitating the need to balance both investment costs and anticipated returns. To achieve this, the goal of maximizing the difference between yearly revenue and investment cost of the EVCS is assessed using the following equation:

$$\max f_1 = F^{\mathrm{s}} - \left(F^{\mathrm{c}} + F^{\mathrm{p}} + F^{\mathrm{om}}\right). \tag{3}$$

1) The yearly EVCS electricity sales cost: The electricity sales cost refers to the annual cost of EVCSs selling electricity to EV users; this is evaluated by using the following equations:

$$F^{\mathrm{s}} = \sum_{j=1}^{N_{\mathrm{EVCS}}} \sum_{t=1}^{T} E_{\mathrm{EVCS}}^{j,t} \times C_{\mathrm{sal}}^t \times D \tag{4}$$

$$E_{\mathrm{EVCS}}^{j,t} = \begin{pmatrix} \left(p_{\mathrm{sl}}^{e,t} + Z_{\frac{\partial}{2}} \times \sigma_{\mathrm{sl}}^t\right) \times N_{\mathrm{sl}}^j \\ + \left(p_{\mathrm{fa}}^{e,t} + Z_{\frac{\partial}{2}} \times \sigma_{\mathrm{fa}}^t\right) \times N_{\mathrm{fa}}^j \end{pmatrix}. \tag{5}$$

2) The yearly EVCS construction cost: The construction cost mainly includes the purchase cost of the EVSEs, fixed cost, and the EVCS land cost. The cost of each charging station's facilities is related to the total number of EVSEs. The fixed cost is the essential expenses required for the construction of the charging station, i.e., the survey, design, construction, and management of the EVCS [48]. The land cost is generally related to the number of EVSE in the EVCS, and the specific layout is shown in Fig. 4. To install a connector, a minimum width of 9' and a length of 18' are required. A minimum clearance of 3' between them is also required if multiple connectors are needed. For each connector, an assumed area requirement of 25 m^2 is stated in this article [49]. The yearly construction cost is the cost allocated to the charging station each year throughout the operating cycle. It is related to the payback period of the EVCS

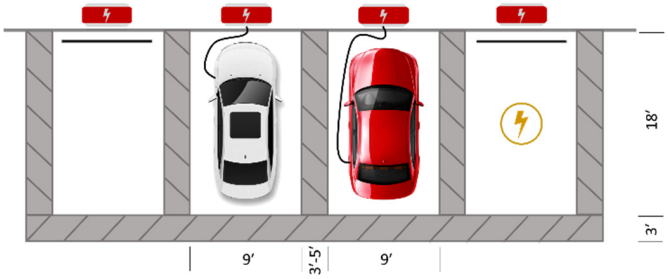

Fig. 4. Layout of EVCS.

and the discount rate, which is expressed as follows:

$$F^{c} = \left(\begin{array}{c} C_{\mathrm{fix}_{\mathrm{cons}}} \\ + \sum_{j=1}^{N_{\mathrm{EVCS}}} \left(P_{\mathrm{EVCS}}^{j} + C_{\mathrm{land}}^{j} \times 25 \times \left(N_{\mathrm{sl}}^{j} + N_{\mathrm{fa}}^{j} \right) \right) \end{array} \right) \times \left(\frac{r(1+r)^{\mathrm{o}}}{(1+r)^{\mathrm{o}} - 1} \right) \tag{6}$$

$$P_{\mathrm{EVCS}}^{j} = N_{\mathrm{sl}}^{j} \times C_{\mathrm{cons_{sl}}} + N_{\mathrm{fa}}^{j} \times P_{\mathrm{fa}} \times C_{\mathrm{cons_{fa}}}. \tag{7}$$

3) The yearly EVCS electricity purchase cost: The yearly electricity purchase cost refers to the cost of purchasing electricity from the grid by the EVCSs each year, as shown in the following equation:

$$F^{\mathrm{p}} = \sum_{j=1}^{N_{\mathrm{EVCS}}} \sum_{t=1}^{T} E_{\mathrm{EVCS}}^{j,t} \times C_{\mathrm{pur}}^{t} \times D. \tag{8}$$

4) The yearly EVCS operating and maintenance costs: The operating and maintenance costs of the charging station mainly include the equipment maintenance and employee wages, which can be converted based on the construction cost of the charging station

$$F^{\mathrm{om}} = \left(\begin{array}{c} C_{\mathrm{fix}_{\mathrm{cons}+}} \\ \sum_{j=1}^{N_{\mathrm{EVCS}}} \left(P_{\mathrm{EVCS}}^{j} + C_{\mathrm{land}}^{j} \times 25 \times \left(N_{\mathrm{sl}}^{j} + N_{\mathrm{fa}}^{j} \right) \right) \end{array} \right) \times (1 + \text{Ü}). \tag{9}$$

B. EV User's Charging Convenience

When planning for EVCSs, it is important to consider both the profitability of the EVCS and the convenience of EV users during charging. To achieve this, we have formulated the objective function f_2 aiming to minimize the combined cost of yearly EV user waiting time and the distance traveled to charge, as depicted in the following equation:

$$\min f_2 = F^{\mathrm{w}} + F^{\mathrm{d}}. \tag{10}$$

1) The yearly EV user waiting time cost: Each EVCS supports two charging modes: slow charging and fast charging. The charging time for slow charging is long, with an average charging time of about 8 h. EV users under this service go about their endeavors once charging starts and return after charging is done; hence, slow charging has no waiting cost. Therefore, the total daily occupancy of slow EVSEs in the jth EVCS is

$$N_{\mathrm{sl}}^{j} = \left\lceil \frac{N_{\mathrm{EV}}^{j} \times \tau_{\mathrm{s}}}{\frac{T_{\mathrm{s}}}{T_{\mathrm{sc}}}} \right\rceil + 1. \tag{11}$$

The average charging time for fast changing is about an hour; the EV user normally waits at the EVCS until charging is complete. Waiting costs are incurred for charging during working hours [50]. Based on [47], most EV users patronize fast charging from 8:00 to 18:00, while few charges outside this range. Therefore, we assume the working hours for estimating fast charge waiting cost as 8:00–18:00.

The EV users' cost of waiting is the time cost incurred due to delays in accessing the charging service. As most users prefer fast charging during working hours, and user income is often calculated based on time, we derive the waiting cost for users from their waiting time, using per capita hourly income as a basis [51]. Building on this premise, we have formulated an objective function to minimize the waiting time cost for EV users, as shown in (12). In addition, to reduce EV users' waiting time without wastage of resources, we have implemented an M/M/S queuing system model as an additional condition, outlined in (13)–(16)

$$F^{\mathrm{w}} = \sum_{j=1}^{N_{\mathrm{EVCS}}} C_{\mathrm{que}} \times W_{\mathrm{que}}^{j} \times N_{\mathrm{EV}}^{j} \times c \times \tau_{\mathrm{f}} \times D \tag{12}$$

$$W_{\mathrm{que}}^{j} = \frac{\left(N_{\mathrm{fa}}^{j} \rho \right)^{N_{\mathrm{fa}}^{j}} \times P_0}{\left(N_{\mathrm{fa}}^{j}! \right)(1-\rho)^2 \times \lambda} \tag{13}$$

$$P_0 = \left[\sum_{k=0}^{N_{\mathrm{fa}}^{j}-1} \frac{\left(\frac{\lambda}{\varepsilon} \right)^{k}}{k!} + \frac{\left(\frac{\lambda}{\varepsilon} \right)^{N_{\mathrm{fa}}^{j}}}{\left(N_{\mathrm{fa}}^{j} \right)!(1-\rho)} \right]^{-1} \tag{14}$$

$$\lambda = \frac{N_{\mathrm{EV}}^{j} \times c \times \tau_{\mathrm{f}}}{T_{\mathrm{f}}} \tag{15}$$

$$\rho = \frac{\lambda}{\varepsilon \times N_{\mathrm{fa}}^{j}}. \tag{16}$$

2) The yearly EV user distance charge cost: As the user travels to the EVCS, their battery power is partially depleted, which is directly linked to the distance between their starting point and the EVCS. The further the distance, the greater the depletion of the battery power, thus resulting in higher charging costs. To quantify this relationship, we convert the driving distance into the distance traveled to charge cost using the following equation:

$$F^{\mathrm{d}} = \sum_{j=1}^{N_{\mathrm{EVCS}}} \sum_{i=1}^{N_{\mathrm{EV}}^{j}} \sqrt{\left(x_j^i - X_j \right)^2 + \left(y_j^i - Y_j \right)^2} \times b \times C_{\mathrm{sal}} \times D. \tag{17}$$

C. Stochastic Stability of System Voltage

EVCSs are typically directly connected to the power grid, and each new station built adds a considerable charging load to the grid. This load can impact voltage stability and even collapse if not managed properly. As a result, maintaining voltage stability is crucial for the safe and reliable operation of the distribution network. Although many studies consider voltage limits a constraint at this stage, they only ensure that the EVCS planning meets the existing requirements. However, with the increasing number of EVs, the EVSE capacity within the EVCS must also expand to meet the rising demand for charging. Therefore, creating an objective function with a voltage limit becomes necessary to allow as many EVs as possible to connect to the grid while maintaining voltage stability.

The conventional method of calculating DPF is not optimal because it fails to consider the random distribution of the network and the time-varying nature of power load, which introduces uncertainty in power flow analysis. We propose an SPF calculation method that combines the cumulants and Gram–Charlier expansion approach to address this. By analyzing the power flow using the probability density function (pdf), we introduce a DSVS index to assess the voltage stability of the power system. Finally, we establish an objective function using the DSVS index to enhance the grid's stability.

1) SPF Formulation: The equations of the grid power injections are as follows [36]:

$$\mathrm{IP} = G(U). \tag{18}$$

When the injected power of node m has a disturbance error at time t, the power equation is expressed as follows:

$$\begin{cases} \Delta W_{m,t} = W_{m,t} - U_{m,t} \sum_{n=1}^{N_{\text{node}}} U_{n,t}(G_{mn}\cos\delta_{mn} + B_{mn}\sin\delta_{mn}) \\ \Delta Q_{m,t} = Q_{m,t} - U_{m,t} \sum_{n=1}^{N_{\text{node}}} U_{n,t}(G_{mn}\sin\delta_{mn} - B_{mn}\cos\delta_{mn}). \end{cases} \tag{19}$$

Equation (20) is expanded according to Taylor Series, ignoring the high-power terms above the second degree, and simplified processing into a linear equation system, as shown in the following equations:

$$\Delta W_{m,t} = J_t \cdot \Delta U_{m,t} \tag{20}$$

$$\Delta W_{m,t} = \Delta W^{\mathrm{L}}_{m,t} + \sum_{j=1}^{N_{\text{EVCS}}} \Delta W^{\text{EVCS}}_{j,m,t} \times B^j_m \tag{21}$$

$$B^j_m = \begin{cases} 1, & \text{if } j \text{ connect the } m \text{ th node} \\ 0, & \text{else} \end{cases} \tag{22}$$

Considering the node injected power $W_{m,t}$ and node voltage $U_{m,t}$ under uncertainty, both can be expressed as two components: expected value and random disturbance

$$W_{m,t} = W^{\mathrm{e}}_{m,t} + \Delta W_{m,t} \tag{23}$$

$$W^{\mathrm{e}}_{m,t} = W^{\mathrm{L}}_{m,t} + \sum_{j=1}^{N_{\text{EVCS}}} W^{\text{EVCS}}_{j,m,t} \times B^j_m \tag{24}$$

$$U_{m,t} = U^{\mathrm{e}}_{m,t} + \Delta U_{m,t}. \tag{25}$$

By combining (18) and (20)–(25), the following two equations can be further obtained:

$$W^{\mathrm{e}}_{m,t} = G\left(U^{\mathrm{e}}_{m,t}\right) \tag{26}$$

$$\Delta U_{m,t} = \left(J_t^{-1}\right) \cdot \Delta W_{m,t}. \tag{27}$$

Let X be a random variable, if $E(X^l)$ $(l = 1, 2, \ldots)$ is exists, then it is called the lth-order raw moment of X, denoted as $a^l(X)$. When the random variable X is discrete, the l-order raw moment $a^l(X)$ is expressed as

$$a^l(X) = E\left(X^l\right) = \sum_{i=1}^{n} p_h x_h^l. \tag{28}$$

According to the functional relationship between the cumulants and the raw moment, the cumulants $K^l(\Delta W_{m,t})$ of the power load and the cumulants $K^l(\Delta U_{m,t})$ of the node voltage can be obtained

$$\begin{cases} K^1\left(\Delta W_{m,t}\right) = a^1\left(\Delta W_{m,t}\right) = \mu, & l = 1 \\ K^l\left(\Delta W_{m,t}\right) = a^l\left(\Delta W_{m,t}\right) \\ \quad - \sum_{j=1}^{l-1} A^j_{l-1} a^j\left(\Delta W_{m,t}\right) K^{l-j}\left(\Delta W_{m,t}\right), & l \geq 2 \end{cases} \tag{29}$$

$$A^j_{l-1} = \frac{(l-1)(l-2)\cdots(l-j)}{j!} \tag{30}$$

$$K^l\left(\Delta U_{m,t}\right) = \left(J_t^{-1}\right)^l \cdot K^l\left(\Delta W_{m,t}\right). \tag{31}$$

After $K^l(\Delta U_{m,t})$ is obtained, the voltage pdf can be obtained by approximating the Gram–Charlier series expansion. In the power system, the Gram–Charlier series can expand the random variable of a distribution function into a series composed of the derivatives of normal random variables. The series coefficient is composed of the cumulants of each random variable. The pdf voltage of the mth node at time t is obtained by the Gram–Charlier series as follows:

$$f\left(\Delta U_{m,t}\right) = \sum_{l=1}^{\infty} C^l\left(\Delta U_{m,t}\right) \varphi^l\left(\Delta U_{m,t}\right). \tag{32}$$

$C^l(\Delta U_{m,t})$ is obtained from $K^l(\Delta U_{m,t})$, as shown in the following equation:

$$\begin{cases} C^0\left(\Delta U_{m,t}\right) = 1 \\ C^1\left(\Delta U_{m,t}\right) = C^2\left(\Delta U_{m,t}\right) = 0 \\ C^3\left(\Delta U_{m,t}\right) = -\dfrac{K^3\left(\Delta U_{m,t}\right)}{\left(K^2\left(\Delta U_{m,t}\right)\right)^{\frac{3}{2}}} \\ C^4\left(\Delta U_{m,t}\right) = \dfrac{K^4\left(\Delta U_{m,t}\right) + 3\left(K^2\left(\Delta U_{m,t}\right)\right)^2}{\left(K^2\left(\Delta U_{m,t}\right)\right)^2} - 3 \\ \vdots \end{cases} \tag{33}$$

2) DSVS Index: According to (29)–(31), the cumulants $K^l(\Delta U_{m,t})$ of the node voltage is obtained as $K^1(\Delta U_{m,t})$ and $K^2(\Delta U_{m,t})$ which are the expectation and the variance of $f(\Delta U_{m,t})$, respectively. From this, the upper and lower voltage boundaries of the mth node at time t can be obtained as follows:

$$U^{\text{upp}}_{m,t} = K^1\left(\Delta U_{m,t}\right) + Z_{\partial/2} * \left|\sqrt{K^2\left(\Delta U_{m,t}\right)}\right| \tag{34}$$

$$U^{\text{low}}_{m,t} = K^1\left(\Delta U_{m,t}\right) - Z_{\partial/2} * \left|\sqrt{K^2\left(\Delta U_{m,t}\right)}\right|. \tag{35}$$

To verify how close the overall pdf of the voltage is to the nominal voltage U^N, we propose a DSVS index. The mth node system voltage stability index at time t is shown in the following equation:

$$I^{\mathrm{DSVS}}(U_{m,t}) = \left(\frac{\left|U_{m,t}^{\mathrm{upp}} - U^{\mathrm{N}}\right|}{U^{\mathrm{N}}} + \frac{\left|U_{m,t}^{\mathrm{low}} - U^{\mathrm{N}}\right|}{U^{\mathrm{N}}} \right) \times 100\%. \tag{36}$$

Since (36) contains absolute values, it is a nonlinear system, not a continuously differentiable function. In nonlinear programming, there are two types of optimal solutions, namely, local and global optimum, and finding the global optimum can be challenging, given the limited time available. On the other hand, in convex programming, there is only one global optimum, and it can be found quickly. To address this problem, a piecewise equation for (36) alleviates the difficulties associated with nonlinearities and helps find the optimal solution more quickly and accurately. Thus, (36) is decomposed into the following equation:

$$I^{\mathrm{DSVS}}(U_{m,t}) = \left(\frac{\beth_{m,t} + \gimel_{m,t}}{U^{\mathrm{N}}} + \frac{\xi_{m,t} + \varrho_{m,t}}{U^{\mathrm{N}}} \right) \times 100\% \tag{37}$$

$$\text{S.t. } \beth_{m,t} = U_{m,t}^{\mathrm{upp}} - U^{\mathrm{N}} \tag{38}$$

$$\gimel_{m,t} = U^{\mathrm{N}} - U_{m,t}^{\mathrm{upp}} \tag{39}$$

$$\xi_{m,t} = U_{m,t}^{\mathrm{low}} - U^{\mathrm{N}} \tag{40}$$

$$\varrho_{m,t} = U^{\mathrm{N}} - U_{m,t}^{\mathrm{low}} \tag{41}$$

$$\beth_{m,t}, \gimel_{m,t}, \xi_{m,t}, \varrho_{m,t} \geq 0. \tag{42}$$

3) Objective Function: In recent years, there has been a significant increase in the number of EVs. The closer the system voltage is to the nominal voltage (U^{N}), the more EVs can be accommodated in the existing EVCS planning, avoiding the need for periodic EVCS replanning. Conversely, as the number of EVs increases, additional EVCSs may be necessary to satisfy the charging demand, thus leading to an increase in EVCS investment costs. To ensure that each node on the power system can remain close to U^{N} at all times, we establish an objective function, as illustrated in the following equation:

$$\min f_3 = \sum_{t=1}^{T} \sum_{m=1}^{N_{\mathrm{node}}} I^{\mathrm{DSVS}}(U_{m,t}). \tag{43}$$

D. Super Efficiency Data Envelopment Analysis

The linear weighting method is a common approach for converting multiobjective programming to a single-objective programming problem. This method involves assigning weights to each objective function to reflect their relative importance in the final outcome. It is essential to determine the appropriate weight coefficient to obtain the desired results [52].

This conversion process can be applied to an economic system or a production process, where a unit produces a certain number of products using a given set of input factors [53], [54]. Although the specifics of these activities may differ, the goal is always to obtain the maximum output using a minimal amount of input. To achieve this objective, a series of decisions need to be made from input to output. These decisions are made by a DMU. Since there are typically many DMUs that seek to maximize their output, it is necessary to evaluate their effectiveness and select the best one as the final decision.

Data envelopment analysis (DEA) is a linear programming-based tool that is specifically designed to assess the relative efficiency of work performance for organizations or projects of the same type. The traditional DEA model, which is used to calculate the effectiveness of the vth DMU, is presented in the following equation:

$$\max\ \vartheta_v = \frac{\sum_{z=1}^{Z} \beta_{v,z} \times y_{v,z}}{\sum_{s=1}^{S} \alpha_{v,s} \times x_{v,s}} \tag{44}$$

$$\text{S.t. } \vartheta_v \leq 1 \tag{45}$$

$$\beta_{v,z}, \alpha_{v,s} \geq 0 \quad \forall z, s. \tag{46}$$

Equations (44)–(46) demonstrate that a more significant value of ϑ_v indicates that the vth DMU can produce more output using less input. A value of $\vartheta_v < 1$ implies that the input exceeds the output, which means that the vth DMU is wasting resources and is, thus, considered ineffective. On the other hand, when $\vartheta_v = 1$, the vth DMU is the most efficient compared to the other DMUs, and no other DMU can use less input to obtain the same output. Typically, there may be several effective DMUs or just one. However, the traditional DEA model cannot accurately identify these effective DMUs.

SEDEA model is a new model proposed based on the traditional DEA model; the difference is that SEDEA model deletes the constraint $\vartheta_v \leq 1$, which excludes the vth DMU from the set of DMUs when evaluating the vth DMU. The efficiency of the original valid DMU value remains unchanged, while the efficiency of the original effective DMU value will be greater than or equal to 1. This way, we can further compare the effective DMU based on the traditional DEA model [55].

In converting a multiobjective programming model to a single-objective programming model, assigning a corresponding weight to each objective function is necessary. Different weight combinations exist, and each can be called DMU. The SEDEA model is used to evaluate the effectiveness of each DMU; finally, we choose the DMU with the most significant value to weigh each objective function in the single-objective programming model. The steps to determining the effective weight coefficient vector are as follows.

Step 1: Normalize three objective functions f_1, f_2, and f_3 in the above model, respectively. The linear weighted sum method transforms the multiobjective problem into a single objective problem, as shown in the following equation:

$$\min\ F = \omega_1 \frac{\max f_1}{f_1} + \omega_2 \frac{f_2}{\min f_2} + \omega_3 \frac{f_3}{\min f_3} \tag{47}$$

$$\text{S.t. } \omega_1 + \omega_2 + \omega_3 = 1 \tag{48}$$

where $\max\ f_1$, $\min f_2$, and $\min f_3$ are the fixed values with respective optimal solutions without considering the other two objective functions; f_1, f_2, and f_3 are the optimal solutions obtained by (47); ω_1, ω_2, and ω_3 are the weight coefficients of $\max\ f_1/f_1$, $f_2/\min f_2$, and $f_3/\min f_3$, respectively.

Step 2: Determine the input and output of the DEA model. The essence of the DEA model is to find the maximum ϑ_v,

that is, to obtain the maximum output with the minimum input. In this article, the objective function f_1 is to obtain the maximum EVCS's benefit, and the objective functions f_2 and f_3, respectively, are to minimize the EV user cost and the voltage deviation rate. Hence, in (47), f_1 is the output value, and f_2 and f_3 are the input values. The following equation is turned into:

$$\min(F_v) = \beta_{v,1}\frac{\max f_1}{f_{v,1}} + \alpha_{v,1}\frac{f_{v,2}}{\min f_2} + \alpha_{v,2}\frac{fv,_3}{\min f_3} \tag{49}$$

$$\text{S.t. } \beta_{v,1} + \alpha_{v,1} + \alpha_{v,2} = 1 \tag{50}$$

where v is the vth DMU; $\beta_{v,1}$ is the weight coefficient of the output of the vth DMU; $\alpha_{v,1}$ and $\alpha_{v,2}$ are the weight coefficients of the input of the vth DMU, respectively; and $f_{v,1}$, $f_{v,2}$, and $f_{v,3}$ are the optimal solutions obtained by the optimization algorithm after the vth input, and output weight vector is brought into (49).

Step 3: We set the step size of the weight coefficient to 0.1 and the weight range of each objective function to 0.1–0.8. According to the permutation and combination methods and their corresponding constraints, there will eventually be 36 weight combinations. The weight combinations matrix is shown in the following equation:

$$\begin{bmatrix} \beta_{1,1} & \alpha_{1,1} & \alpha_{1,2} \\ \beta_{2,1} & \alpha_{2,1} & \alpha_{2,2} \\ \vdots & \vdots & \vdots \\ \beta_{v,1} & \alpha_{v,1} & \alpha_{v,2} \end{bmatrix} = \begin{bmatrix} 0.1 & 0.1 & 0.8 \\ 0.1 & 0.2 & 0.7 \\ \vdots & \vdots & \vdots \\ 0.8 & 0.1 & 0.1 \end{bmatrix}, \quad v = 1, 2, \ldots, 36. \tag{51}$$

Select the vth weight vector in order and substitute it into (50), and (49) is used to obtain the optimal solutions of $f_{v,1}$, $f_{v,2}$, and $f_{v,3}$. Use (44)–(46) to calculate the relative efficiency of the vth DMU based on $f_{v,1}$, $f_{v,2}$, and $f_{v,3}$.

Step 4: Repeat Step 3 until the efficiency values of all 36 groups are obtained. Finally, select the weight vector corresponding to the DMU whose ϑ is the highest as the multiobjective function for weighting.

E. Constraints

1) System power flow constraints

$$\begin{cases} W_m = U_m \sum_{n=1}^{N_{\text{node}}} U_n (G_{mn}\cos\delta_{mn} + B_{mn}\sin\delta_{mn}) \\ Q_m = U_m \sum_{n=1}^{N_{\text{node}}} U_n (G_{mn}\sin\delta_{mn} - B_{mn}\cos\delta_{mn}). \end{cases} \tag{52}$$

2) Node voltage amplitude constraint

$$U^{\min} \le U_{m,t}^{\text{low}} < U_{m,t}^{\text{upp}} \le U^{\max}. \tag{53}$$

3) Power constraints of EVCSs access points

$$\left(N_{\text{sl}}^j \times P_{\text{sl}} + N_{\text{fa}}^j \times P_{\text{fa}}\right) \times B_m^j \le P_{m,t}^{\max}. \tag{54}$$

4) Service radius constraint.

One of the key factors to consider when planning for EVCS is the range of service provided by the station. This range is directly linked to the distance between the users' starting point and the charging station. As the service radius increases, the capacity of the charging station to provide service decreases. Hence, the service radius is subject to the following constraint:

$$\sqrt{\left(x_j^i - X_j\right)^2 + \left(y_j^i - Y_j\right)^2} \le R_{\max}. \tag{55}$$

1) Charging queuing time constraint: To prevent inefficient use of resources, the maximum waiting time for EV users to charge their vehicles should satisfy the following conditions:

$$W_{\text{que}}^j \le W_q^{\max}. \tag{56}$$

2) Constraints on the number of EVSEs in each EVCS: According to [56], the construction of each EVCS must have more than three EVSEs, so the number of EVSEs in each charging station is restricted as follows:

$$N_{\text{sl}}^j + N_{\text{fa}}^j \ge 3. \tag{57}$$

3) EV user charging requirement constraints: To meet the charging requirement of EV users, the rated capacity of the jth EVCS should be greater than the total EV charging requirement within the service range

$$\sum_{t=1}^{T} E_{\text{EVCS}}^{j,t} \le N_{\text{sl}}^j \times P_{\text{sl}} \times T_{\text{s}} + N_{\text{fa}}^j \times P_{\text{fa}} \times T_{\text{f}}. \tag{58}$$

IV. Joint Solution Method Combining Voronoi Diagram and ADEOA

A. Voronoi Diagram

The voronoi diagram is an effective mathematical and geometric tool with broad applications in various fields due to its efficiency, intuitive space allocation, and partitioning capabilities [57]. Its primary use lies in the substation site selection and service scope division in power systems. Since the location problem of EVCS shares similarities with that of substations, this study uses the voronoi diagram to identify the optimal location. The voronoi diagram is a geometric shape formed by expanding each point set G at the same rate until they meet. Each seed on the plane corresponds to a unique voronoi cell or polygon. Any point within the voronoi polygon is closer to its nucleus than any other seed.

Set $G = \{G_1, G_2, \ldots, G_n\}$, $3 \le n \le \infty$ that is a set of seeds on the plane, and then, the Voronoi diagram can be defined as [58]

$$\text{V}(G_u) = \left\{x \in V(G_u) | d(x, G_u) \le d\left(x, G_j\right)\right\}. \tag{59}$$

With N_{EVCS} as the number of EVCS, the entire area can be divided into N_{EVCS} subareas using (59). Each subarea represents the service range of an EVCS, ensuring that the distance from each EV within the service range to its corresponding EVCS is shorter than the distance to other EVCSs.

B. Adaptive Differential Evolution Optimization Algorithm

The ADEOA is a random parallel heuristic search algorithm [59] that follows specific rules for selection, crossmutation, and iteration from a random group. It aims to evaluate individuals based on a fitness function, retain good ones, and eliminate inferior ones to guide the search process toward the optimal solution. Additionally, ADEOA uses adaptive mutation operators to preserve helpful information and prevent the destruction of the optimal solution. As a result, this algorithm dramatically increases the likelihood of finding the global optimum solution.

The ADEOA algorithm requires fewer parameter adjustments compared to other optimization algorithms. Furthermore, the optimization results are not influenced by the parameter settings. It is especially effective in dealing with high-dimensional problems and offers fast convergence and high accuracy. For these reasons, we have chosen to utilize ADEOA to solve the model presented in this article. Fig. 5 shows the flowchart for the EVCS siting and sizing method, which follows the solution process outlined below.

Step 1: Input data—randomly generate the location and charging behavior of each EV, the baseload profile, the baseload fluctuation range, and the basic system parameters of the distributed grid.

Step 2: Determine the number N of EVCS in the planning area. In this article, we assume $N \in$ [4, 10].

Step 3: Use the ADEOA algorithm to randomly initialize the locations of N charging stations and the number of fast EVSEs in each EVCS.

Step 4: Use (59) to divide the service range of charging stations and connect each EVCS to the nearest grid node. Since there is no queuing problem for slow charging, it is only necessary to use (11) to determine the number of slow EVSEs required based on the number of EVs that need slow charging within the service range of each EVCS.

Step 5: Calculate the yearly profit of EVCS (f_1) and the annual charging cost of EV users (f_2) by using (3)–(9) and (10)–(17), respectively.

Step 6: Calculate the stability of the system voltage (f_3).

Step 6.1: Set $t = 1$.

Step 6.2: Set the grid node $m = 1$.

Step 6.3: Input the expected value of the injected power $W^{e}_{m,t}$ at time t based on (24) and through (26) to calculate the node voltage $U^{e}_{m,t}$ and the Jacobian matrix J_t in the expected state.

Step 6.4: Calculate the l-order raw moment of injected power ($a^l(\Delta W_{m,t})$) based on (28).

Step 6.5: Use (29)–(31) to obtain the lth cumulant moment of the power load $K^l(\Delta W_{m,t})$ and node voltage $K^l(\Delta U_{m,t})$.

Step 6.6: Use (32)–(33) expand to get the probability distribution function of node voltage $f(\Delta U_{m,t})$.

Step 6.7: Check whether the current grid node m is equal to N^{node}, if so, continue to the the next step; otherwise, $m = m+ 1$, return to Step 6.3.

Step 6.8: Check whether the current time t is equal to T, if so, continue to the next step; otherwise, $t = t + 1$,return to Step 6.2.

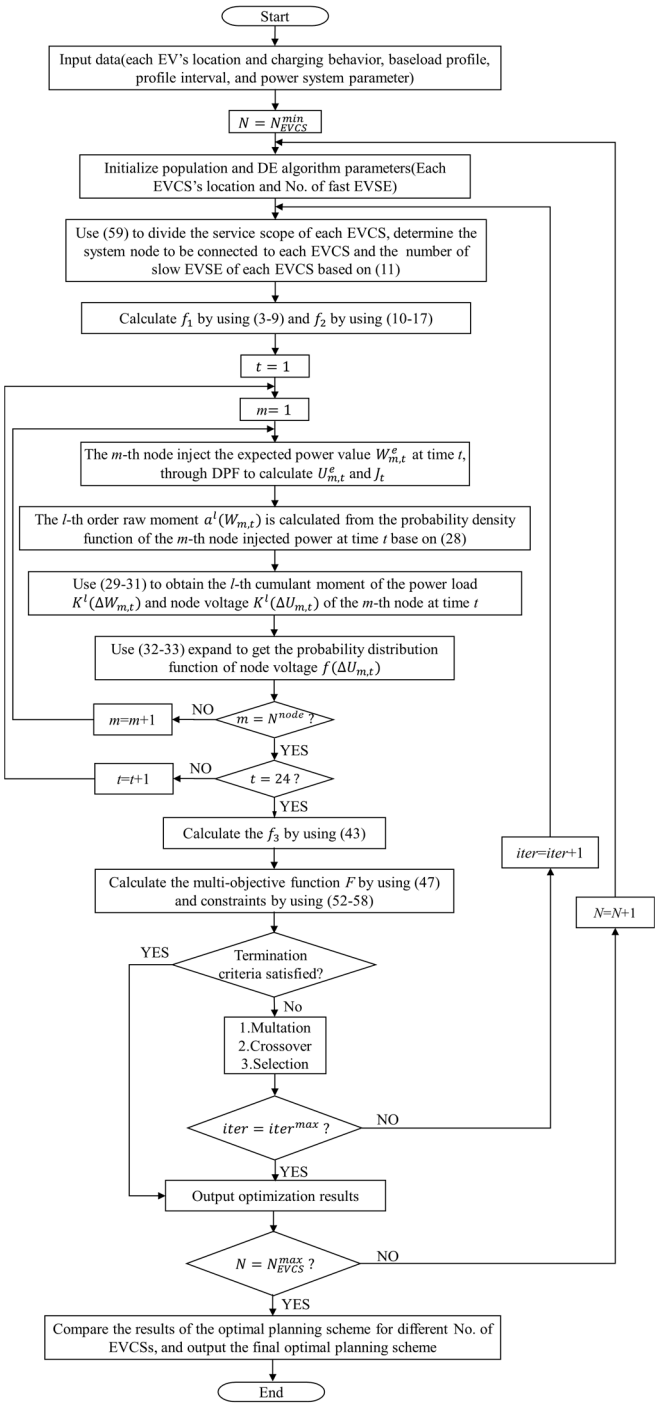

Fig. 5. Flowchart for EVCS siting and sizing method.

Step 6.9: Calculate the stochastic stability of the system voltage (f_3) by using (43).

Step 7: Calculate the multiobjective function F by using (47) and constraints by using (52)–(58).

Step 8: Check whether the termination condition is satisfied, if so, turn to Step 11; otherwise, continue to the next step.

Step 9: Perform mutation and crossover operations on the population to obtain the experimental population, and the algorithm selects a better population from the original population and the experimental population as the new population through the greedy selection criterion.

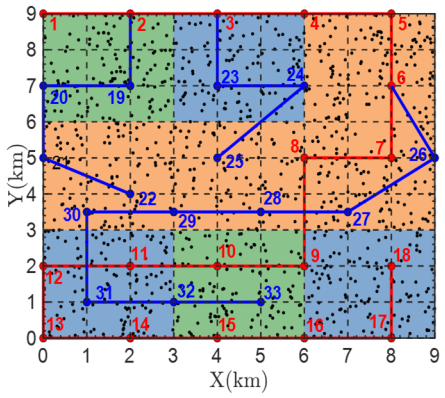

Fig. 6. Planning diagram.

Step 10: Check whether the current iteration iter is equal to $\text{iter}^{\max}$, if so, the optimal global solution at this time is the optimal charging station planning scheme when the number of EVCSs is N, and continue to the next step; otherwise, iter $=$ iter $+ 1$, return to Step 4.

Step 11: Calculate the results of the optimal planning scheme when the number of EVCSs is N.

Step 12: Check whether the current number N of EVCSs is equal to $N_{\text{EVCS}}^{\max}$, if so, compare the results of the optimal planning scheme for different numbers of EVCSs, and output the final optimal planning scheme; otherwise, set $N = N + 1$ and return to Step 3.

V. Case Study

In this study, the planning area was set to be 81 m^2 and divided into nine subareas based on their load types. The IEEE 33-node distribution network system topology diagram was also considered, as illustrated in Fig. 6. The orange, green, and blue areas represent the commercial, residential, and industrial loads. Meanwhile, blue and red dots denote the branch and trunk branch nodes in the IEEE 33-node distribution network. This article uses our previous work [60] to predict the mean and deviation values of the injection power on each node. Each EV's location is indicated by a black dot, while blue solid and red lines represent the branches and trunks, respectively.

This study considered 1000 EVs with varying types and battery capacities in the planning area. There are 18 EV models under consideration, each with battery capacity, as listed in Table I. Based on the approach outlined in Section II, this study formulated probability models for both fast and slow EV charging, with the corresponding results in the following figures. Fig. 7 depicts the probability of charging power modeled for slow charging, revealing a charging power range of 5.9–7 kW, with relatively lower power output observed from 9:00 to 16:00. In Fig. 8, the probability of charging power modeled for fast charging is presented, demonstrating scattered charging power from 0:00 to 5:00, while the average power at other times is around 30 kW. The overall charging power at any given moment can be calculated by utilizing the number of slow and fast EVSEs of each EVCS, as depicted in (5). The time-of-use (TOU) price under consideration is shown in Table II [61], [62].

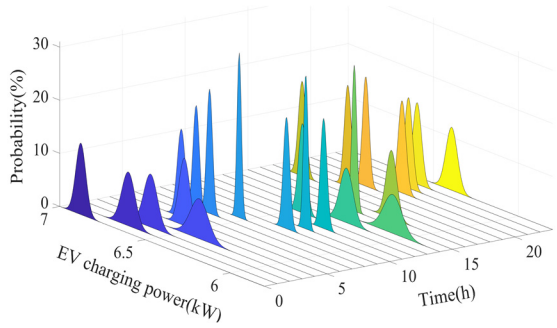

Fig. 7. Probability charging power model of slow charging mode.

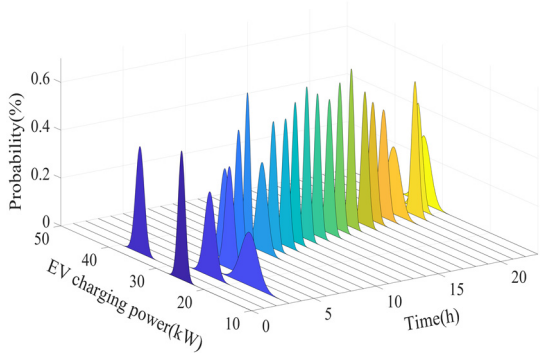

Fig. 8. Probability charging power model of fast charging mode.

TABLE II
TOU Price

	Time	C_{pur}($/kWh)	C_{sal}($/kWh)
On-peak	16:00-21:00	0.2154	0.59
Partial-peak	8:00-16:00, 21:00-0:00	0.17297	0.49
Off-peak	0:00-8:00	0.14296	0.39

We assume the following during the planning process: 1) users will use the nearest EVCS and travel via the shortest path; 2) there are no parking space limitations in the queue around each EVCS; and 3) every EVCS is connected to its nearest grid node. The necessary parameters for the case study are presented in Table III [48], [63], [64], [65], [66], [67], [68].

A. Selection of Weight Coefficient

Three objective functions were considered individually in the planning area with five EVCSs. The maximum yearly profit of EVCS was U.S. $5 844 200, the minimum annual charging cost for EV users was U.S. $314 600, and the system's minimum dynamic voltage stability index was 2856. Table IV presents the relative efficiency of each weight vector according to the method described in Section III-D.

Table IV shows that the DEA efficiency of each weight is evaluated as [0.1, 0.1, 0.8] and [0.5, 0.3, 0.2], which sum to 1. To select the best weight set, we use the SEDEA model to compare these two weights further. According to the results, the relative efficiency of the weight vector [0.1, 0.1, 0.8] has the highest SEDEA value, that is, given the input f_2 and f_3 when each weight vector is the same, the output f_1 with a weight vector [0.1, 0.1, 0.8] is the highest. Therefore,

TABLE III
OPTIMIZE MODEL PARAMETERS

Symbol	Parameter	Value
r	Discount rate	0.1
o	Payback period	20(year)
C_{cons_sl}	Construction cost of each slow EVSE	540.07($)
C_{cons_fa}	Unit power construction cost for each fast EVSE	77.15($/kW)
C_{fix_cons}	Fixed construction cost	153600($)
C_{land}	Residentail land price	458($/m^2)
	Commercial land price	645($/m^2)
	Industrial land price	603($/m^2)
P_{sl}	Charging power for slow charger	7(kW)
P_{fa}	Charging power for fast charger	50(kW)
D	Days per year	365
T	Time	24
υ	Conversion factor	0.2
b	Average EV energy consumption per km	0.15(kWh/km)
C_{que}	Queuing time cost for EV user	3.88($)
c	EV charging times per day	0.5
ε	Average system service rate	2
τ_f	The proportion of users choosing fast charging	0.8
τ_s	The proportion of users choosing slow charging	0.2
T_{sc}	Average charging duration time for slow charging	8
T_f	Working hours for fast charging mode	11
T_s	Working hours for slow charging mode	24
η	Charging efficiency	0.9

TABLE IV
DEA AND SEDEA MODEL RESULTS

Weight	f_1	f_2	f_3	DEA	SEDEA
[0.1,0.1,0.8]	3879107.75	437111.6	3135.6	1	1.026
[0.1,0.8,0.1]	3879107.75	434739.4	3498.9	0.952	0.952
[0.5,0.3,0.2]	4079083.54	425301.5	3342.8	1	1
[0.7,0.2,0.1]	4122683.1	451413.4	3599.6	0.948	0.948

[0.1, 0.1, 0.8] is selected as the final weight vector of the objective function.

B. Optimization Results of the Siting and Sizing of EVCSs

The quantity of EVCSs under consideration falls within the planned range of 4–10. Fig. 9(a) shows the final optimal objective function value F under different numbers of EVCSs, which follows a parabolic trend. When the weights of the objective functions are [0.1, 0.1, 0.8], the smallest values of the objective function are achieved with five EVCSs. Fig. 9(b) presents the optimal values of f_1, f_2, and f_3 for different numbers of EVCSs. As shown in Fig. 9(b), increasing the number of EVCSs leads to a higher yearly profit for EVCSs (f_1) and a lower annual charging cost for EV users (f_2). The stochastic stability of the system voltage (f_3) shows a nonlinear trend, with the lowest value observed when there are five EVCSs in the planned area. Therefore, considering all factors, it is reasonable to establish five EVCSs within the planning area.

Fig. 10 shows each location of the five EVCSs under consideration. The service range of each EVCS is divided by the voronoi diagram, and Fig. 10 shows that the EVCSs are almost evenly distributed in the area. In Fig. 11, the grid

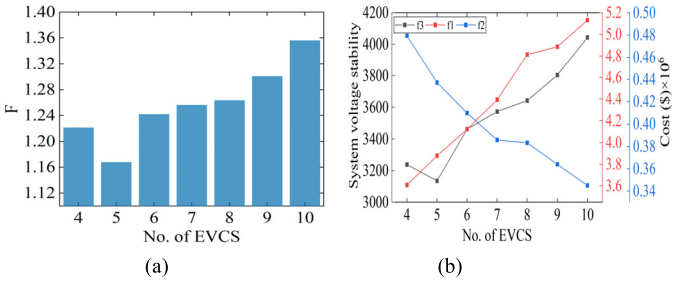

Fig. 9. Optimal results of objective functions under different number of EVCS: (a) F and (b) f_1, f_2, and f_3.

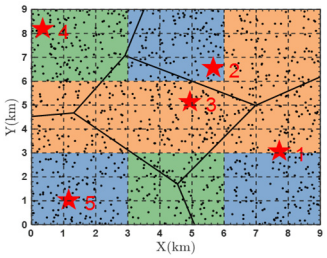

Fig. 10. Location and service range of each EVCS.

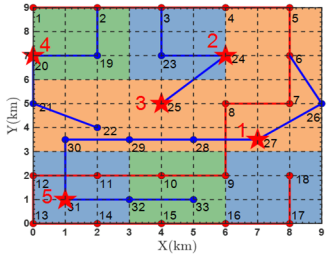

Fig. 11. Grid nodes to be connected to each EVCS.

TABLE V
CONFIGURATION AND OPERATION PARAMETERS OF EACH EVCS

	EVCS1	EVCS2	EVCS3	EVCS4	EVCS5
W_q(min)	4.05	6.41	5.64	6.96	5.94
λ	9	8	7.77	6.27	7.86
ρ(%)	64.29	66.67	64.77	62.73	65.53
N_{fa}	7	6	6	5	6
N_{sl}	7	6	7	4	6
N_{EV}	232	206	207	156	199

nodes that connect to each EVCS are shown. The EVCSs are connected to the grid's 27th, 24th, 25th, 20th, and 31th nodes, respectively.

Table V presents the configuration and operation of each EVCS. As shown in Table V, the waiting time at each EVCS is less than 7 min, indicating that EV users are provided with better service. The value of ρ (%) represents the fraction of the service capacity used, showing that the charger utilization rate of each EVCS is more than 62.73%. Therefore, the proposed scheme's optimization results improve the convenience of EV users by providing charging at a lower cost. Table V also displays the EVs serviced at each EVCS and the corresponding number of fast and slow EVSEs.

To solve the proposed model, this article sets the termination error value, maximum number of iterations, and population

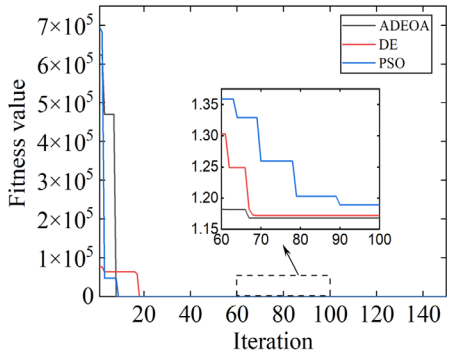

Fig. 12. Convergence curves for ADEOA, DE, and PSO.

TABLE VI
PLANNING RESULT UNDER DIFFERENT CONFIDENCE INTERVELS

	85%	90%	95%
Access point	17,19,24,8,22	27,2,6,29,22	27,24,25,20,31
N_{fa}	5,6,6,6,7	7,6,6,5,6	7,6,6,5,6
N_{slow}	6,5,6,7,8	8,4,7,6,6	7,6,7,4,6
$F^c + F^{om}$	304287.83	301694.14	294783.80
F^p	3050279.9	3291792.06	3652155.12
F^s	6536314.194	7053840.135	7826046.674
F^w	368039.09	381930.3	390992.22
F^d	46535.232	46244.68	46119.364
f_1	3181746.4	3460354	3879108
f_2	414574.32	428175	437111.6
f_3	3160.9	3145.1	3135.6

size in the ADEOA algorithm to be 1E-6, 150, and 50, respectively. To evaluate the effectiveness of the ADEOA algorithm, this study conducts a comparative analysis with differential evolution (DE) and particle swarm optimization (PSO) [69], and the iterative process of the three algorithms is illustrated in Fig. 12. As seen from Fig. 12, ADEOA exhibits the fastest convergence speed, achieving optimization and the best fitness value in the 68th iteration. Although DE completes the optimization at the 69th iteration with a similar convergence speed to ADEOA, the fitness value obtained is greater. In contrast, PSO exhibits the slowest convergence speed, completing optimization at the 90th iteration and obtaining the biggest fitness value. In conclusion, ADEOA outperforms the other two algorithms regarding convergence speed and accuracy, making it more suitable for solving the proposed model in this article.

C. Sensitivity Analysis

This section examines the sensitivity of an EVCS planning model to different confidence levels, EV penetrations, and land prices.

Table VI displays the optimization results of EVCS planning under various confidence levels when the number of EVCSs in the planning area is five. Table VI demonstrates that as the confidence level increases, the number of slow EVSEs also gradually decreases the construction cost (F^{c}) and operating costs (F^{om}) of the EVCS decline as the number of EVSEs decreases. The expenses incurred from purchasing electricity (F^{p}) and electricity sales (F^{s}) are primarily influenced by the number of EVSEs and the charging power of EVs, increasing in both F^{p} and F^{s} with higher confidence levels. The value of EVCS profit (f_1) demonstrates an increase of 8.75% and 21.92% for 90% and 95% confidence levels, respectively, compared to 85%. Table VI also reveals a gradual increase in the waiting time cost (F^{w}) and a gradual decrease in the distance traveled to charge cost (F^{d}) with an increase in confidence level. Furthermore, the overall EV user cost (f_2) increases gradually as the confidence interval rises, with the value of f_2 increasing by 3.28% and 5.43% for 90% and 95% confidence levels, respectively, compared to the value under the 85% confidence level. Finally, comparing the values of overall voltage deviation (f_3) across different confidence levels reveals that the value of f_3 decreases by 0.499% and 0.8% for 90% and 95% confidence levels, respectively, compared to the value under the 85% confidence level.

TABLE VII
PLANNING RESULT UNDER DIFFERENT EV PENETRATIONS

	0%	150%	200%
Access point	27,24,25,20,31	24,27,33,22,19	32,24,26,19,33
N_{fa}	7,6,6,5,6	10,7,7,9,7	9,13,9,11,8
N_{slow}	7,6,7,4,6	9,10,5,10,7	12,11,9,13,8
f_1	3879108	5187220.394	6504557.339
Avef_2	437.1115795	440.61458	447.349856
f_3	3135.6	3592.64	4271.99

Table VII displays the optimization results of EV charging station planning under various EV penetrations when there are five EVCSs in the planning region. According to Table VII, the EV penetration rate influences the planning outcomes of EVCSs. The total cost of F^{w} and F^{d} grows as the quantity of EVs increases. It is challenging to analyze the impact of different EV penetration rates on EV users using f_2 alone; hence, this article employs the average user cost (Ave $f_2 = f_2/N_{\mathrm{EV}}$).

As the number of EVs grows, so does the number of EVSEs required in the EVCSs. This results in increased operating expenses for the operator and more significant earnings. The value of f_1 increases by 33.72% and 67.68% at 150% and 200% EV penetration rates, respectively, compared to 0%. The average user charging cost rises in tandem with the rate of EV uptake. In particular, average user costs rise by 0.801% and 2.34% at 150% and 200% EV penetration rates, respectively, compared to 0%. Yet, as the number of EVs increases, so does the grid's injected power, thus resulting in a rise in the voltage deviation rate (f_3). Table VII illustrates that as EV penetration rates grow, so does the value of f_3. Notably, for 150% and 200% EV penetration rates, the f_3 values rise by 14.57% and 36.24%, respectively, compared to a 0% EV penetration rate.

In Fig. 13, the planning results assume equal land prices for different land uses. As depicted, three EVCSs are constructed on commercial land, and two EVCSs are built on industrial land. However, in Fig. 11, two EVCSs are erected on commercial land, two on industrial land, and one on residential land. Specific planning outcomes under various land prices are displayed in Table VIII. Notably, when land prices are equal, the total number of EVSEs is 61, one more than the practical land prices scenario. Furthermore, compared to practical land prices, the values of f_1, f_2, and f_3 are reduced by 3.13%, 1.25%, and 2.58%, respectively, when land prices are equal.

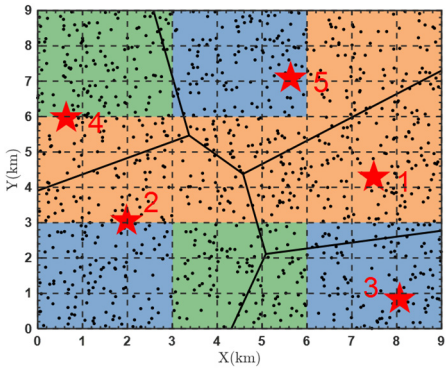

Fig. 13. Location and service under uniform land pricing.

TABLE VIII
PLANNING RESULT UNDER SPECIFIC LAND PRICES

	Practical Pricing	Unifrom pricing
Access point	27,24,25,20,31	7,22,17,21,24
N_{fa}	7,6,6,5,6	6,7,4,5,7
N_{slow}	7,6,7,4,6	6,8,5,5,8
f_1	3879108	3757529
f_2	437111.6	431622.7
f_3	3135.6	3054.55

In summary, various degrees of confidence have a more significant impact on operator revenue and EV user costs but have less effect on power grid stability. However, various EV penetration rates significantly influence operator profitability and grid stability but have a minor impact on EV user costs. Assuming the uniform land price is more advantageous to both EV users and the grid in charging station planning, while considering practical land prices benefits operators more.

D. Case Comparasion

In order to validate the model presented in this article, the authors compared it with methods proposed in [27] and [31]. These articles also considered the uncertainty associated with EVs. Zeb et al. [27] used a DPF calculation method, while Pal et al. [31] used a probabilistic power flow calculation method based on the two-point estimation algorithm. Comparing the outcomes of the three models showed that the proposed approach is effective.

This section presents the results of comparing the proposed method for EVCS planning with two other methods (from [27] and [31]) that also consider the uncertainty of EVs. The comparison is made based on the optimization results of charging station planning under different methods when the number of EVCSs in the planning area is 5.

Table IX presents the charging station planning optimization results using various methods considering five EVCSs in the planning region. Table IX shows that the total number of EVSEs ($N_{\text{fa}} + N_{\text{slow}}$) acquired via [31] is 31, whereas the total number of EVSEs produced via the proposed method and that of [27] is 30. As a result, the f_1 value of [31] rises by 0.263% compared to the proposed method and [27]. From the perspective of the EV user, the proposed approach achieves the highest value for objective function, which is an

TABLE IX
PLANNING RESULT UNDER VARIOUS METHODS

	Proposed method	[31]	[27]
Access point	27,24,25,20,31	4,19,2,32,18	9,19,30,6,2
N_{fa}	7,6,6,5,6	6,6,4,7,7	7,5,7,7,4
N_{slow}	7,6,7,4,6	7,7,3,6,8	8,4,7,7,4
f_1	3879108	3889360	3879108
f_2	437111.6	434238.8	433584.3
f_3	3135.6	3428.43	3547.561

increase of 0.66% and 0.81% compared to the methods by [31] and [27], respectively. Regarding power grid stability, the proposed method has the lowest value for objective function, which is a drop of 8.54% and 11.61% compared to the methods by [31] and [27], respectively.

In summary, the planning outcome achieved using various power flow methodologies has less influence on operators and EV customers but has a more significant impact on grid stability. Applying the proposed method increases power grid stability while protecting the interests of operators and EV consumers, demonstrating the proposed method's effectiveness.

To further prove the robustness of the proposed model, this article analyzes the voltage change of the proposed method and that of [27] under different baseload and EV penetrations.

Fig. 14 shows the voltage fluctuation profile under different baseload and EV penetrations obtained using the proposed method. The black dotted line represents the minimum allowable voltage offset value, set to be 0.9 p.u. The red solid line and the red shades indicate the average voltage and its fluctuation range when the distribution line only has the baseload. The blue solid line and the blue shades show the average voltage and its fluctuation range when the distribution line has both the baseload and 1000 EVs. The yellow solid line and the yellow shades display the average voltage and its fluctuation range when the distribution line has 150% penetration of baseload and 1500 EVs. The green solid line and the green shades represent the average voltage and its fluctuation range when the distribution line has a 200% penetration of baseload and 2000 EVs.

It can be seen from Fig. 14(a) that the voltage at 9:00 in a day is the lowest. When there is only the baseload connected to the distribution line, the fluctuation range of the lowest voltage is [0.954, 0.965], which is much larger than the voltage 0.9 p.u., so the voltage stability of the system far meets the requirements. When the EVs are connected to the grid, the voltage range is [0.942, 0.953]; the highest voltage offset is 5.8%; and the lowest voltage offset is 4.7%, which is still within the allowable range of the voltage offset. When the baseload and EV penetration increase by about 180%, the node voltage range will be lower than the voltage limit, and the EVCS needs to be replanned.

Fig. 14(b) shows the voltage fluctuation profile of all nodes at 9:00 under different baseload and EV penetrations obtained using the SPF method. When EV penetration gradually increases, the EVSE in each EVCS increases accordingly. Fig. 14 reveals that the voltage deviation increases in the IEEE 33-node distribution network as the distance between

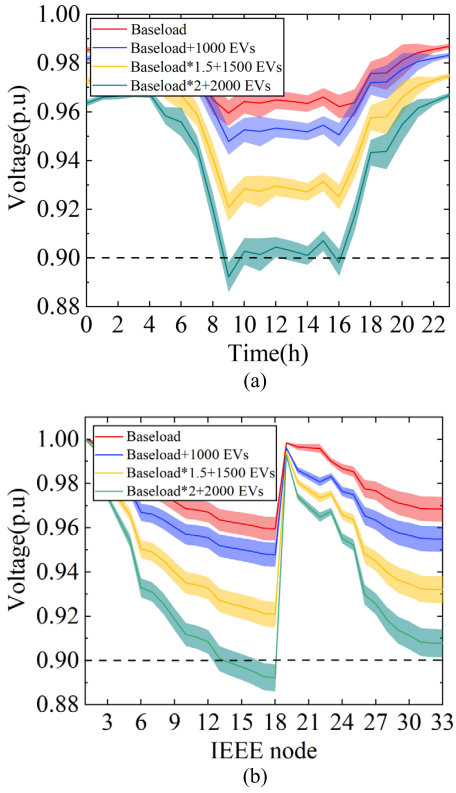

Fig. 14. Voltage profile under different baseload and EV penetrations obtained by the proposed method: (a) voltage profile of node 18 and (b) voltage profile of all nodes at 9:00.

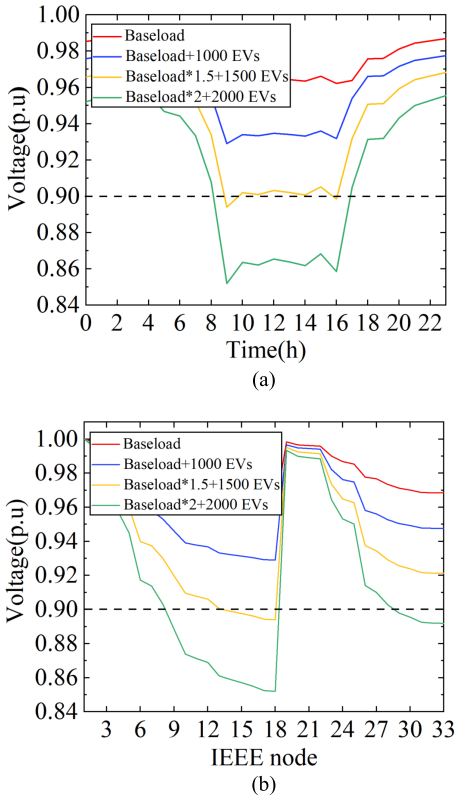

Fig. 15. Voltage profile under different baseload and EV penetrations obtained by Zeb et al. [27]: (a) voltage profile of node 18 and (b) voltage profile of all nodes at 9:00.

a node and the first node increases. With only the baseload on the distribution line, the voltage at the 18th node exhibits the lowest value, ranging between 0.954 and 0.965 p.u. This range is significantly within the voltage threshold of 0.9 p.u., indicating that the system's voltage stability well satisfies the necessary criteria. When the baseload and EV penetration increase to about 180%, the voltage ranges of the 13th–18th nodes are lower than the voltage limit, while the voltage ranges of other nodes are still within the voltage limit.

Fig. 15(a) shows the voltage profile of node 18 under different baseload and EV penetrations as presented in [27]. Similar to Fig. 14(a), the voltage at 9:00 is the lowest. When only the baseload is present in the grid, the lowest voltage is 0.959 p.u., corresponding to a voltage offset of 4.1% for node 18. When EVs connect to the grid, the voltage in Fig. 15(a) drops to 0.9238 p.u., and the voltage offset increases to 7.62%. Compared to the proposed method, the voltage offset rate of [27] has increased by 19.32%. Although it can accommodate the current number of EVs, it is very close to the maximum allowable voltage offset. When the baseload and EV penetration increase to about 145%, the node voltage drops below the acceptable voltage limit. However, the proposed method still keeps the voltage offset within the allowable range, and it does not exceed the range of voltage offset until EV penetration increases to 180%.

Fig. 15(b) depicts the voltage profiles of all nodes at 9:00 under different baseload and EV penetrations obtained by Zeb et al. [27]. Fig. 15(b) shows a voltage transition at terminal node 18. At node 18, when only the baseload is linked to the distribution line, the voltage measures 0.959 p.u. When the EVs are connected to the grid, the voltage in Fig. 15(b) decreases to 0.9238 p.u. When the penetration increases to about 145%, the voltages of nodes 13–18 and 29–33 fall below the voltage limit, while the voltages of other nodes remain higher than the voltage limit. Compared with the proposed method, both the voltage offset rate and the number of nodes beyond the voltage offset range in [27] increase significantly. Through the comparison, it can be seen that the method proposed in this article can accommodate more EVs and is more robust.

VI. Conclusion

This article establishes a comprehensive optimization model of EVCS site and size planning, which considers the benefits of the operators, EV users, and the influence of the distribution network's uncertainties. In addition, we use the SEDEA method to select the weight of each objective function in the optimization model and use the voronoi diagram and the ADEOA to solve the model jointly. Finally, the proposed method is verified and analyzed using the IEEE-33 node power distribution system as a case study.

It can be seen from Table V that for the five EVCSs, the average waiting time of EV users does not exceed 7 min. The EVCSs provide EV users with better services, and the utilization rate of the chargers at the EVCS is more than 62.73%. Based on satisfying EV users with high-quality services, the EVCSs have been well-utilized.

Comparing the proposed method with other power flow calculation methods for EVCS planning, it is evident that the proposed method can improve the stability of the power

grid while ensuring the interests of operators and EV users. For the proposed method, when 1000 EVs are connected to the grid, the voltage range is [0.942, 0.953], which is much larger than the voltage 0.9 p.u., so the voltage stability of the system far meets the requirements. When the baseload and EV penetration increase to about 180%, the node voltage range will be lower than the voltage limit. For [27], when the baseload and EV penetration increase to about 145%, the node voltage will be lower than the voltage limit.

In summary, the proposed method for siting and sizing planning of EVCSs is more viable and justifiable. It can efficiently enhance the EVCS's profit, improve the charging convenience for EV users, and ensure the stability of the system voltage. This method is a significant reference for future EVCS planning.

In future research, we aim to incorporate traffic network factors and a dynamic interception location model to improve the convenience of EV users.

REFERENCES

[1] J. Kim and H. Oh, "Robust operation scheme of EV charging facility with uncertain user behavior," *IEEE Trans. Ind. Informat.*, early access, Jan. 2023.

[2] X. Hao, Y. Chen, H. Wang, H. Wang, Y. Meng, and Q. Gu, "A V2G-oriented reinforcement learning framework and empirical study for heterogeneous electric vehicle charging management," *Sustain. Cities Soc.*, vol. 89, Feb. 2023, Art. no. 104345.

[3] Finance & economics. (2020). *Charging Piles Are Advancing Wildly: Many Places Are Built to Get Subsidies, and Now They Are Abandoned and Wasteful*. [Online]. Availiable: https://baijiahao.baidu.com/s?id=1683605821988561O&wfr=spider&for=pc

[4] S. F. Kong et al., "Two-stage robust planning model and its solution algorithm of active distribution network containing electric vehicle charging stations," *Trans. China. Electrotechnical Soc.*, vol. 35, no. 5, pp. 1093–1105, Mar. 2020.

[5] S. Ge et al., "Optimal deployment of electric vehicle charging stations on the highway based on dynamic traffic simulation," *Trans. China. Electrotechnical Soc.*, vol. 33, no. 13, pp. 2991–3001, Jul. 2018.

[6] J. Ugirumurera and Z. J. Haas, "Optimal capacity sizing for completely green charging systems for electric vehicles," *IEEE Trans. Transport. Electrific.*, vol. 3, no. 3, pp. 565–577, Sep. 2017.

[7] D. Yan and C. Ma, "Optimal sizing of a PV based electric vehicle charging station under uncertainties," in *Proc. 45th Annu. Conf. IEEE Ind. Electron. Soc.*, Lisbon, Portugal, vol. 1, Oct. 2019, pp. 4310–4315.

[8] A. Hussain, V.-H. Bui, and H.-M. Kim, "Optimal sizing of battery energy storage system in a fast EV charging station considering power outages," *IEEE Trans. Transport. Electrific.*, vol. 6, no. 2, pp. 453–463, Jun. 2020.

[9] L. Luo, Z. Wu, W. Gu, H. Huang, S. Gao, and J. Han, "Coordinated allocation of distributed generation resources and electric vehicle charging stations in distribution systems with vehicle-to-grid interaction," *Energy*, vol. 192, Feb. 2020, Art. no. 116631.

[10] G. Zhou, Z. Zhu, and S. Luo, "Location optimization of electric vehicle charging stations: Based on cost model and genetic algorithm," *Energy*, vol. 247, May 2022, Art. no. 123437.

[11] H. Duan et al., "Coordinated planning for electric vehicle charging station and distribution network considering time-of-use charging price," in *Proc. CSU-EPSA*, Jan. 2017, vol. 29, no. 1, pp. 103–110.

[12] X. Guo, X. Zhang, J. Dong, and X. Yang, "Optimal allocation of urban new energy vehicles and traditional energy vehicles considering pollution and cost," *Environ., Develop. Sustainability*, Feb. 2023.

[13] D. Ji, M. Lv, J. Yang, and W. Yi, "Optimizing the locations and sizes of solar assisted electric vehicle charging stations in an urban area," *IEEE Access*, vol. 8, pp. 112772–112782, 2020.

[14] H. Parastvand, O. Bass, M. Masoum, Z. Moghaddam, S. Lachowicz, and A. Chapman, "Placement and sizing of EV charging stations according to centrality of the underlying network," in *Proc. Intermountain Eng. Technol. Comput. (IETC)*, Orem, UT, USA, Oct. 2020, pp. 1–6.

[15] J. Chen et al., "EV charging station planning based on travel demand," *Elec. Power. Autom. Equipment.*, vol. 36, no. 6, pp. 34–39, Jun. 2016.

[16] X. Liu and Z. Bie, "Optimal allocation planning for public EV charging station considering AC and DC integrated chargers," *Energy Procedia*, vol. 159, pp. 382–387, Feb. 2019.

[17] X. Ren, H. Zhang, R. Hu, and Y. Qiu, "Location of electric vehicle charging stations: A perspective using the grey decision-making model," *Energy*, vol. 173, pp. 548–553, Apr. 2019.

[18] Z. Zhu, Z. Gao, J. Zheng, and H. Du, "Charging station planning for plug-in electric vehicles," *J. Syst. Sci. Syst. Eng.*, vol. 27, no. 1, pp. 24–45, Jul. 2017.

[19] S. Deb, X.-Z. Gao, K. Tammi, K. Kalita, and P. Mahanta, "A novel chicken swarm and teaching learning based algorithm for electric vehicle charging station placement problem," *Energy*, vol. 220, Apr. 2021, Art. no. 119645.

[20] S. N. Hashemian, M. A. Latify, and G. R. Yousefi, "PEV fast-charging station sizing and placement in coupled transportation-distribution networks considering power line conditioning capability," *IEEE Trans. Smart Grid*, vol. 11, no. 6, pp. 4773–4783, Nov. 2020.

[21] Y. Zhang, Y. Wang, F. Li, B. Wu, Y. Chiang, and X. Zhang, "Efficient deployment of electric vehicle charging infrastructure: Simultaneous optimization of charging station placement and charging pile assignment," *IEEE Trans. Intell. Transp. Syst.*, vol. 22, no. 10, pp. 6654–6659, Oct. 2021.

[22] O. Erdinc et al., "Optimal sizing and siting of distributed generation and EV charging stations in distribution systems," in *Proc. ISGT-Europe*, Turin, Italy, Sep. 2017, pp. 1–9.

[23] S. Wang, Z. Y. Dong, F. Luo, K. Meng, and Y. Zhang, "Stochastic collaborative planning of electric vehicle charging stations and power distribution system," *IEEE Trans. Ind. Informat.*, vol. 14, no. 1, pp. 321–331, Jan. 2018.

[24] A. Awasthi, K. Venkitusamy, S. Padmanaban, R. Selvamuthukumaran, F. Blaabjerg, and A. K. Singh, "Optimal planning of electric vehicle charging station at the distribution system using hybrid optimization algorithm," *Energy*, vol. 133, pp. 70–78, Aug. 2017.

[25] S. Negarestani, M. Fotuhi-Firuzabad, M. Rastegar, and A. Rajabi-Ghahnavieh, "Optimal sizing of storage system in a fast charging station for plug-in hybrid electric vehicles," *IEEE Trans. Transport. Electrific.*, vol. 2, no. 4, pp. 443–453, Dec. 2016.

[26] L. F. Henrique, W. N. Silva, C. C. A. Silva, B. H. Dias, L. W. Oliveira, and M. C. D. Almeida, "Optimal siting and sizing of distributed energy resources in a smart campus," *Electric Power Syst. Res.*, vol. 217, Apr. 2023, Art. no. 109095.

[27] M. Z. Zeb et al., "Optimal placement of electric vehicle charging stations in the active distribution network," *IEEE Access*, vol. 8, pp. 68124–68134, 2020.

[28] M. H. Amini, M. P. Moghaddam, and O. Karabasoglu, "Simultaneous allocation of electric vehicles' parking lots and distributed renewable resources in smart power distribution networks," *Sustain. Cities Soc.*, vol. 28, pp. 332–342, Jan. 2017.

[29] M. A. Kazemi, M. Sedighizadeh, M. J. Mirzaei, and O. Homaee, "Optimal siting and sizing of distribution system operator owned EV parking lots," *Appl. Energy*, vol. 179, pp. 1176–1184, Oct. 2016.

[30] V. H. Fan, Z. Dong, and K. Meng, "Integrated distribution expansion planning considering stochastic renewable energy resources and electric vehicles," *Appl. Energy*, vol. 278, Nov. 2020, Art. no. 115720.

[31] A. Pal, A. Bhattacharya, and A. K. Chakraborty, "Allocation of electric vehicle charging station considering uncertainties," *Sustain. Energy, Grids Netw.*, vol. 25, Mar. 2021, Art. no. 100422.

[32] H. Wang, Z. Yan, X. Xu, and K. He, "Probabilistic power flow analysis of microgrid with renewable energy," *Int. J. Electr. Power Energy Syst.*, vol. 114, Jan. 2020, Art. no. 105393.

[33] Z. Zhang et al., "Probabilistic evaluation of voltage quality in distribution networks considering the stochastic characteristic of distributed generators," in *Proc. CSEE*, vol. 33, no. 13, 2013, pp. 150–156.

[34] H. Zhang and P. Li, "Probabilistic analysis for optimal power flow under uncertainty," *IET Gener., Transmiss. Distribution*, vol. 4, no. 5, p. 553, 2010.

[35] X. Lin et al., "An unscented transformation based probabilistic power flow for autonomous hybrid AC/DC microgrid with correlated uncertainty sources," in *Proc. 2nd IEEE Conf. Energy Internet Energy System Integr. (EI2)*, Oct. 2018, pp. 1–6.

[36] P. Wei, J. Liu, Q. Zhou, J. Chen, and N. Zhang, "Research on impact of prediction error of new energy on power grid based on probabilistic power flow algorithm," in *Proc. IEEE 2nd Int. Conf. Big Data Anal. (ICBDA)*, Mar. 2017, pp. 573–577.

[37] X. Li, B. Li, and L. Zhang, "Molding the impact of all-electric suburbs on power grids using probabilistic load flow," in *Proc. IEEE 3rd Int. Conf. Power Data Sci. (ICPDS)*, Dec. 2021, pp. 1–6.

[38] X. Guo, M. Zhou, S. Liu, and L. Qi, "Lexicographic multiobjective scatter search for the optimization of sequence-dependent selective disassembly subject to multiresource constraints," *IEEE Trans. Cybern.*, vol. 50, no. 7, pp. 3307–3317, Jul. 2020.

[39] C. Xu, X. Liu, E. Wang, Y. Zheng, and S. Wang, "Rockburst prediction and classification based on the ideal-point method of information theory," *Tunnelling Underground Space Technol.*, vol. 81, pp. 382–390, Nov. 2018.

[40] L. Jiao, J. Luo, R. Shang, and F. Liu, "A modified objective function method with feasible-guiding strategy to solve constrained multi-objective optimization problems," *Appl. Soft Comput.*, vol. 14, pp. 363–380, Jan. 2014.

[41] R. Jing et al., "A multi-objective optimization and multi-criteria evaluation integrated framework for distributed energy system optimal planning," *Energy Convers. Manage.*, vol. 166, pp. 445–462, Jun. 2018.

[42] S. Cheng and Z. Li, "Multi-objective network reconfiguration considering V2G of electric vehicles in distribution system with renewable energy," *Energy Procedia*, vol. 158, pp. 278–283, Feb. 2019.

[43] P. G. Panah, S. M. Bornapour, S. M. Nosratabadi, and J. M. Guerrero, "Hesitant fuzzy for conflicting criteria in multi-objective deployment of electric vehicle charging stations," *Sustain. Cities Soc.*, vol. 85, Oct. 2022, Art. no. 104054.

[44] J. García-Villalobos, I. Zamora, K. Knezović, and M. Marinelli, "Multi-objective optimization control of plug-in electric vehicles in low voltage distribution networks," *Appl. Energy*, vol. 180, pp. 155–168, Oct. 2016.

[45] L. Bitencourt, T. P. Abud, B. H. Dias, B. S. M. C. Borba, R. S. Maciel, and J. Quirós-Tortós, "Optimal location of EV charging stations in a neighborhood considering a multi-objective approach," *Electric Power Syst. Res.*, vol. 199, Oct. 2021, Art. no. 107391.

[46] Q. Liu, J. Liu, and D. Liu, "Intelligent multi-objective public charging station location with sustainable objectives," *Sustainability*, vol. 10, no. 10, p. 3760, Oct. 2018.

[47] Y. Jin, B. Yu, M. Seo, and S. Han, "Optimal aggregation design for massive V2G participation in energy market," *IEEE Access*, vol. 8, pp. 211794–211808, 2020.

[48] T. Z. Yan et al., "Optimal planning of electric vehicle charging station based on PSOSA algorithm," *Electr. Meas. Instrumentation.*, vol. 54, no. 6, pp. 11–16, Mar. 2017.

[49] P. Sadeghi-Barzani, A. Rajabi-Ghahnavieh, and H. Kazemi-Karegar, "Optimal fast charging station placing and sizing," *Appl. Energy*, vol. 125, pp. 289–299, Jul. 2014.

[50] F. Varshosaz, M. Moazzami, B. Fani, and P. Siano, "Day-ahead capacity estimation and power management of a charging station based on queuing theory," *IEEE Trans. Ind. Informat.*, vol. 15, no. 10, pp. 5561–5574, Oct. 2019.

[51] H. J. Cui and Y. P. Li, "Optimization method for opening number of lanes based on operating costs of toll station and queuing costs of driver," *Highway*, vol. 4, pp. 149–152, Apr. 2013.

[52] S. Cheng et al., "Optimal planning of charging stations for electric vehicles considering voltage stability of distribution system and the quality of service," *Power Syst. Protection Control*, vol. 47, no. 7, pp. 12–21, Apr. 2019.

[53] D. J. Wang et al., "Relative efficiency of extended black-start restoration plans based on super efficiency data envelopment analysis model," *Electric Power Autom. Equipment.*, vol. 35, no. 2, Feb. 2015.

[54] G. Wang, Z. Xu, F. Wen, and K. P. Wong, "Traffic-constrained multiobjective planning of electric-vehicle charging stations," *IEEE Trans. Power Del.*, vol. 28, no. 4, pp. 2363–2372, Oct. 2013.

[55] A. A. Noura, F. H. Lotfi, G. R. Jahanshahloo, and S. F. Rashidi, "Super-efficiency in DEA by effectiveness of each unit in society," *Appl. Math. Lett.*, vol. 24, no. 5, pp. 623–626, May 2011.

[56] *Code for Design of EV Charging Stations GB50966-2014*, China Planning Press, China, 2014.

[57] X. Feng and A. T. Murray, "Allocation using a heterogeneous space Voronoi diagram," *J. Geographical Syst.*, vol. 20, no. 3, pp. 207–226, Jul. 2018.

[58] W. Lee, R. Schober, and V. W. S. Wong, "An analysis of price competition in heterogeneous electric vehicle charging stations," *IEEE Trans. Smart Grid*, vol. 10, no. 4, pp. 3990–4002, Jul. 2019.

[59] K. Price, *Differential Evolution*. Cham, Switzerland: Springer, 2005.

[60] Y. Jin, M. A. Acquah, M. Seo, and S. Han, "Short-term electric load prediction using transfer learning with interval estimate adjustment," *Energy Buildings*, vol. 258, Mar. 2022, Art. no. 111846.

[61] *EVgo*. Accessed: Jun. 2022. [Online]. Available: https://www.evgo.com/pricing/tou/

[62] *Pacific Gas & Electric*. Accessed: Jun. 2022. [Online]. Available: https://www.pge.com/tariffs/assets/pdf/tariffbook/ELEC_SCHEDS_B-19.pdf

[63] J. Y. Guan et al., "Optimal allocation of charging stations considering stochastic charging behavior and low carbon efficiency of electric vehicles," *Electr. Power Sci. Technol.*, vol. 34, no. 4, pp. 93–100, Dec. 2019.

[64] F. Baouche, R. Billot, R. Trigui, and N.-E. El Faouzi, "Efficient allocation of electric vehicles charging stations: Optimization model and application to a dense urban network," *IEEE Intell. Transp. Syst. Mag.*, vol. 6, no. 3, pp. 33–43, Jul. 2014.

[65] H. Liu, "Determination of location of electrical vehicle charging stations based on the hybrid algorithm that based on particle swarm optimization and genetic algorithm and capacity optimization," M.S. thesis, Dept. Electron. Eng., Xi'an Univ. Technol., Xi'an, China, 2016.

[66] *Manhattan Industrial Market Trends*. Accessed: Jul. 2022. [Online]. Available: https://www.propertyshark.com/mason/market-trends/industrial/nyc/manhattan

[67] *Manhattan Commercial Market Trends*. Accessed: Jul. 2022. [Online]. Available: https://www.propertyshark.com/mason/market-trends/commercial/nyc/manhattan

[68] (2022). *Data: The Price Per Square Foot for Homes Has Quadrupled Since 1980*. [Online]. Available: https://homebay.com/price-per-square-foot-2022/

[69] B. Yang et al., "Comprehensive overview of meta-heuristic algorithm applications on PV cell parameter identification," *Energy Convers. Manage.*, vol. 208, Mar. 2020, Art. no. 112595.

Yuwei Jin (Member, IEEE) received the M.Sc. degree from the School of Electrical Engineering, Northeast Electric Power University (NEEPU), Jilin, China, in 2017, and the Ph.D. degree in electrical and electronic engineering from Kyungpook National University, Daegu, South Korea, in 2023.

She is currently a Post-Doctoral Researcher of Electrical and Electronic Engineering with Kyungpook National University. Her research interests include smart grid, vehicle-to-grid (V2G), energy management systems, machine learning, and system optimization.

Moses Amoasi Acquah (Member, IEEE) received the B.Sc. and M.Phil. degrees in computer engineering from the University of Ghana, Accra, Ghana, in 2011 and 2014, respectively, and the Ph.D. degree in electrical engineering from Kyungpook National University, Daegu, South Korea, in 2018.

He is currently an Assistant Professor with Keimyung University, Daegu. His research interests include energy management systems, vehicle-to-grid systems, big data, the Internet of Things (IoT), machine learning, and system optimization.

Mingyu Seo (Student Member, IEEE) received the B.Sc. degree from the Department of Electrical Engineering, Yeungnam University, Gyeongsan, South Korea, in 2018, and the M.Sc. degree in electrical and electronic engineering from Kyungpook National University, Daegu, South Korea, in 2020, where he is currently pursuing the Ph.D. degree in electrical and electronic engineering.

His research interests include energy management system, electric vehicle (EV) scheduling, and electricity markets.

Sekyung Han (Member, IEEE) received the B.Sc. degree in electrical engineering and computer science from Hanyang University, Seoul, South Korea, in 2002, the M.Sc. degree from the School of Electrical Engineering and Computer Science, Seoul National University, Seoul, in 2007, and the Ph.D. degree in information science from The University of Tokyo, Tokyo, Japan, in 2012.

He is currently an Associate Professor with Kyungpook National University, Daegu, South Korea. His research interest is system optimization, battery storage technology, energy network, energy management, and electric vehicles.